

AIRFLOW AND WOOD DRYING MODELS FOR WOODKILNS

By

Zhengbing Bian

B. Eng., Huazhong University of Science & Technology, China, 1996

A THESIS SUBMITTED IN PARTIAL FULFILLMENT OF
THE REQUIREMENTS OF THE DEGREE OF
MASTER OF APPLIED SCIENCE
in
THE FACULTY OF GRADUATE STUDIES
DEPARTMENT OF MECHANICAL ENGINEERING

We accept this thesis as conforming
to the required standard

THE UNIVERSITY OF BRITISH COLUMBIA

May 2001

© Zhengbing Bian, 2001

In presenting this thesis in partial fulfillment of the requirements for an advanced degree at the University of British Columbia, I agree that the library shall make it freely available for reference and study. I further agree that permission for extensive copying of this thesis for scholarly purposes may be granted by the head of my department or by his or her representatives. It is understood that copying or publication of this thesis for financial gain shall not be allowed without my written permission.

Department of Mechanical Engineering
The University of British Columbia
2324 Main Mall
Vancouver, BC
Canada V6T 1Z4

Date: May 1, 2001

Abstract

Airflow and heat/mass transfer in a woodkiln are simulated numerically. The uniformity of drying and the quality of the wood in a kiln are strongly influenced by the airflow. A numerical model that simulates the airflow distribution is described and applied to solve the flow distribution in a kiln. The influences of the gaps between lumber pieces and the unevenness of lumber height on the velocity distribution and heat/mass transfer in the woodkiln are investigated numerically. A mathematical model for heat and mass transfer during the wood drying process is presented. The influence of kiln temperature, humidity and transport properties of wood is numerically investigated. The three key parameters in the model are moisture content M , temperature T and total pressure P in the gaseous phase. The results are compared with drying rate experiments carried out by Forintek Canada Corporation. Numerical model predictions are in satisfactory agreement with experimental results. Airflow and wood drying models are coupled to carry out a complete calculation. The model will constitute a powerful tool to optimize kiln design and to help operators improve kiln operations without entailing major new costs.

TABLE OF CONTENTS

ABSTRACT	ii
LIST OF TABLES	v
LIST OF FIGURES	vi
ACKNOWLEDGEMENTS	ix
CHAPTER 1 INTRODUCTION	1
1.1 IMPORTANCE FOR STUDYING WOOD DRYING	1
1.2 WOOD DRYING PROCESS DESCRIPTION	3
1.3 WOOD STRUCTURE.....	5
1.4 CONTRIBUTIONS OF THE RESEARCH WORK	6
CHAPTER 2 AIRFLOW MODELLING	7
2.1 IMPORTANCE OF AIRFLOW IN THE WOODKILN	7
2.2 FACTORS THAT AFFECT AIRFLOW	8
2.3 AIRFLOW INSIDE A TYPICAL WOODKILN	12
2.4 MODELLING OF THE GAPS AND BOARD IRREGULARITIES	18
CHAPTER 3 WOOD DRYING MODELLING	23
3.1 OVERVIEW OF THE VARIOUS WOOD DRYING MODELS	23
3.2 WOOD DRYING MODEL BASED ON WATER-POTENTIAL.....	25
3.3 MATHEMATICAL MODEL.....	27
3.3.1 <i>Equations governing timber drying</i>	28

3.3.2 <i>Boundary Conditions</i>	32
3.3.3 <i>Sub-model used in the simulation</i>	33
3.3.4 <i>Equilibrium Moisture Content</i>	35
3.4 RESULTS AND DISCUSSIONS.....	37
3.4.1 <i>Description of drying process</i>	40
3.4.2 <i>Effect of transport parameters</i>	44
CHAPTER 4 COUPLING OF AIRFLOW AND WOOD DRYING MODELS... 51	
4.1 WHY THE COUPLING PROCESS IS NEEDED	51
4.2 COUPLING PROCESS DESCRIPTION	51
4.3 MESSAGE PASSING INTERFACE (MPI)	57
4.3.1 <i>Collective Communications</i>	58
4.4 RESULTS AND DISCUSSIONS.....	60
CHAPTER 5 CONCLUSIONS AND RECOMMENDATIONS..... 72	
5.1 CONCLUSIONS.....	72
5.2 RECOMMENDATIONS FOR FUTURE WORK	74
APPENDIX: COEFFICIENTS AND PROPERTY CORRELATIONS 76	
NOMENCLATURE..... 79	
REFERENCES..... 82	

LIST OF TABLES

Table 1.1: Approximate Air-Drying Periods for 2.5-cm Lumber.....	2
Table 1.2: Typical Softwood Kiln-Drying Time Schedules for 2.5-cm Ponderosa Common Pine.....	3
Table 3.1: Different Wood Drying Models.	24

LIST OF FIGURES

Figure 1.1: Diagram of Drying Kiln	3
Figure 1.2: Drying Curve.....	4
Figure 1.3: Cross section of tree trunk.....	5
Figure 2.1: Sources of Airflow Variations.....	9
Figure 2.2: Effect of Package Unevenness	11
Figure 2.3: Simulated Kiln Geometry.....	13
Figure 2.4: Computational Mesh for 30° Roof.....	14
Figure 2.5a: Airflow in a typical woodkiln.....	15
Figure 2.5b: Contour Plot of “U”.....	16
Figure 2.5c: Contour Plot of “V”.....	16
Figure 2.5d: Contour Plot of the Pressure.....	17
Figure 2.6: A Proposed Airflow Distribution	17
Figure 2.7: Layout of a typical flow situation	18
Figure 2.8: Grid layout of the simulation	19
Figure 2.9: Shear stress distribution	21
Figure 2.10: Velocity Distribution.....	22
Figure 3.1: Moisture content-water potential relationship of western hemlock sapwood along the boundary desorption and absorption curves at 21 °C (From A. Cloutier 1991)	25

Figure 3.2: Boundary Condition	32
Figure 3.3: The evaporative front model for drying of a softwood board.	34
Figure 3.4: Locations of the selected wood pieces	37
Figure 3.5: Moisture content at different Y as a function of drying time (Case 1)	38
Figure 3.6: Average moisture content as a function of drying time (Case 1,2 and 3).....	39
Figure 3.7: Average temperature as a function of drying time (Case 1,2 and 3).....	39
Figure 3.8: Average moisture content as a function of drying time (case 4).....	42
Figure 3.9: Average moisture content as a function of drying time (case 5).....	42
Figure 3.10: Moisture Content Distribution at Different Drying Times (case 1).....	45
Figure 3.11: Moisture Content Distribution at Different Drying Times (case 3).....	46
Figure 3.12: Pressure Distribution at Different Drying Times (case 1).....	47
Figure 3.13: Pressure Distribution at Different Drying Times (case 3).....	48
Figure 3.14: Temperature Distribution at Different Drying Times (case 1).....	49
Figure 3.15: Temperature Distribution at Different Drying Times (case 3).....	50
Figure 4.1: Illustration of the coupling process	52
Figure 4.2: MPI and Computer System	57
Figure 4.3: Collective Communication.....	59
Figure 4.4: Simulated Wood Kiln.....	60
Figure 4.5: Temperature inside a typical woodkiln at different times.....	61
Figure 4.6: Temperature along the centerline of each channel (3D-Surface).....	62
Figure 4.7: Temperature along the centerline of each channel (2D-Contour).....	62

Figure 4.8: Shear stress at the boundary	63
Figure 4.9: Shear Stress at Channel Top.....	64
Figure 4.10: Shear Stress at Channel Bottom	64
Figure 4.11: Heat Transfer Coefficient at Channel Top	65
Figure 4.12: Heat Transfer Coefficient at Channel Bottom.....	65
Figure 4.13: Average moisture content distribution	66
Figure 4.14: Average temperature distribution.....	67
Figure 4.15: Moisture Content Distribution for No. 1, 12, 28 and 40	68
Figure 4.16: Moisture Content Distribution for No. 60, 84, 87 and 110	69
Figure 4.17: Temperature in Flow Field Reversal Case	71

Acknowledgements

I would like to thank my supervisors, Dr. Martha Salcudean and Dr. Ian Gartshore, for their advice and our many discussions. I would like to thank Dr. Eric Bibeau for discussions on the topic of airflow in wood kilns. I would also like to thank Forintek Canada Corp., especially Dr. Luiz Oliveira, and Canfor Forest Products for their support and discussions with various wood kiln operators. I would like to acknowledge the financial assistance from NSERC and Canfor.

Finally, I would like to express my gratitude to my wife Zheqiong Wang. Her consideration and encouragement made my research work possible.

Chapter 1 Introduction

1.1 Importance for Studying Wood Drying

Wood is an important natural resource, one of the few that are renewable. It is prevalent in our everyday lives and in the economy, in wood-frame houses and furniture; newspapers, books, and magazines; bridges and railroad ties; and organic chemicals. Wood supplies the solid raw material for products, such as lumber, and the fibre for paper, paperboard. Many wood products can be recovered for reuse or recycling, thus extending our wood supply into the future.

Up to 75% of the weight of green wood is water. Nearly all the physical properties of wood are significantly influenced by its moisture content. Most of this water must be removed during processing in order to improve its mechanical and structural properties and decrease the cost of transportation. When wood is well dried, subsequent shrinking and swelling are minimal, making further cutting and machining easier and more efficient. Drying is also an efficient way to prevent degradation due to biological activity, since wood with less than a 22 percent moisture content is immune to fungal attack. A number of methods are available for drying lumber, ranging from air and kiln drying to special seasoning processes. The moisture content goal for air-drying is approximately 20%. The advantages of air-drying are the low initial cost and energy saving. However, it takes a very long time to dry lumber to a desired moisture content, especially in regions with no suitable weather conditions (see Table 1.1 and 1.2). Although in many places in the world wood is still dried by exposing it to atmospheric conditions, the wood dry kiln,

which provides a controllable environment, is becoming more commonplace. According to a survey taken during the 1990s, approximately 85 percent of the overall lumber production in the United States was kiln dried [40].

Table 1.1: Approximate Air-Drying Periods for 2.5-cm Lumber

Species	Days Required to Air-dry to 20%
Baldcypress	100-300
Hickory	70-200
Magnolia	60-150
Oak	
Red	100-300
white	150-300
Pine, southern	40-150
Sweet gum	70-300
Sycamore	70-200
Tupelo	70-200
Yellow poplar	60-150

Drying is the most energy consuming and yet the least understood part of the lumber manufacturing process. For quite a long time, industrial timber drying kilns were designed based only on experience and trial and error. It is necessary to develop formal methods for designing kilns to meet the increasing need to dry lumber quickly while ensuring minimal lumber degradation and energy consumption. There are two mechanisms in the wood drying process: the internal process of the heat and mass transfer inside the lumber, and the external process of the heat and mass transfer at the lumber and airflow interface. To date, there have been very few mathematical models to

simulate these two processes simultaneously for lumber population inside the commercial kiln. Existing work has focused separately on the airflow and the wood drying [2, 7-9, 15, 16, 30-38]. This research work aims to extend the scope of the existing work.

Table 1.2: Typical Softwood Kiln-Drying Time Schedules for 2.5-cm Ponderosa Common Pine

Hours in Kiln	Dry-bulb Temperature, °C	Wet-bulb Temperature, °C	Relative Humidity, %
Heartwood			
1-8	54	43	52
8-16	58	44	48
16 until dry	60	44	41
Sapwood			
1-12	54	43	52
12-24	58	44	48
24 until dry	60	44	41

1.2 Wood Drying Process Description

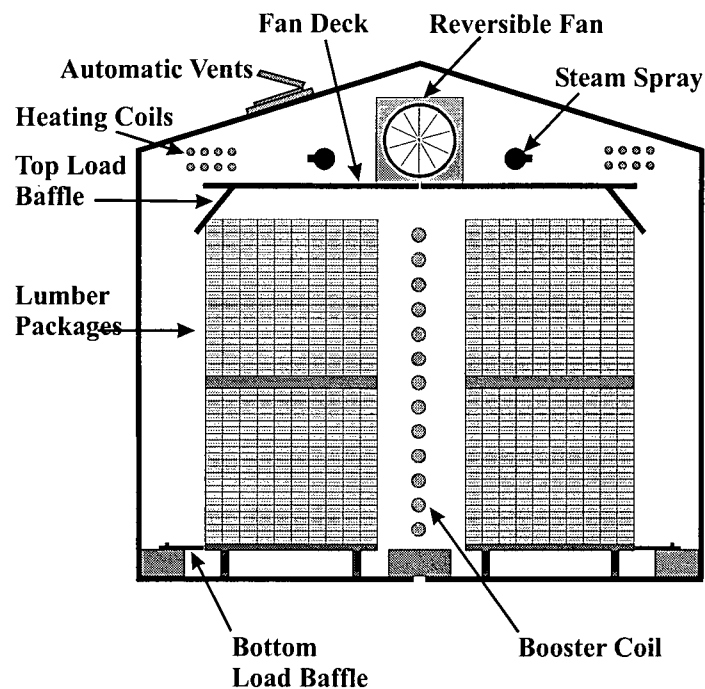


Figure 1.1: Diagram of Drying Kiln

A typical wood kiln, shown diagrammatically in Figure 1.1, provides control over the temperature, humidity, and air circulation for drying lumber. An optimized kiln should remove water inside the wood in the least amount of time to a desired moisture content and with a low moisture variation, while utilizing the least amount of energy, and avoiding wood drying defects which can occur during convection drying [26,14]. Drying defects - rupture of wood tissues, checking, warping, discoloration and uneven moisture content - account for a large cost in kiln operation. Kiln operators must try to achieve uniform drying both within a load and within a lumber piece. They must increase the profitability of their operation by reducing costs associated with excess energy consumption and loss of grade caused by defects resulting from improper drying.

Currently, lumber drying is still based mainly on empirical knowledge. In order to optimize this process, kiln control systems based on models of simultaneous heat and mass transfer in wood during drying have to be developed. The mechanism of drying can be divided into three different stages as shown in Figure 1.2 (stage I is very short, since the free water at the surface is removed very quickly). Good wood drying models should be able to simulate all three stages.

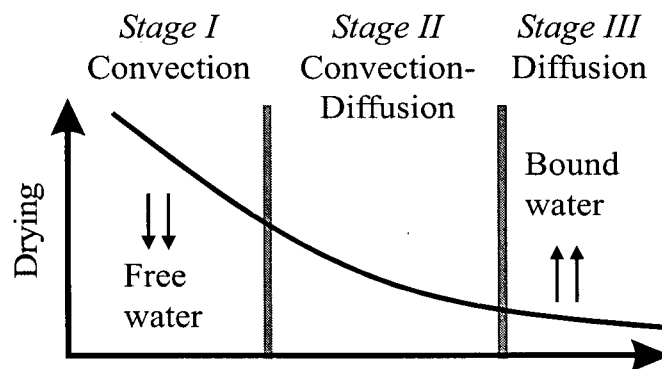


Figure 1.2: Drying Curve

1.3 Wood Structure

Trees are either hardwoods or softwoods. Hardwood trees generally have broad leaves, and are porous, i.e., they contain vessel elements and they are found in the temperate regions of the world. Softwood trees generally have scalelike or needlelike leaves, and are nonporous, i.e., they do not contain vessel elements. The structure of hardwoods is more complex than that of softwoods because more cell types are present in hardwoods. In this paper, only the drying of softwood was investigated.

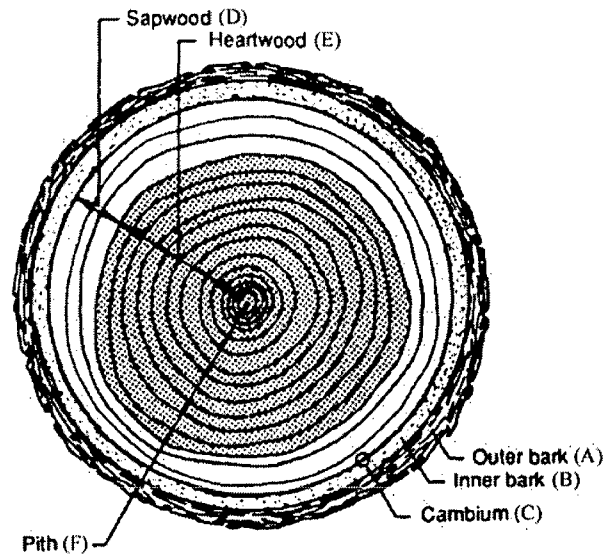


Figure 1.3: Cross section of tree trunk

A cross section of a tree is shown in Figure 1.3. From the outermost to the center are bark, which may be divided into an outer dead part (A), and an inner thin living part (B), which carries food from the leaves to growing parts of the tree, and then three zones of wood, which are differentiated into sapwood (D), heart-wood (E) and pith (F). The wood rays (G) connect various layers from pith to bark for storage and transfer of food. The cambium layer (C), which is inside the inner bark and forms wood and bark cells, can be

seen only with a microscope. These cells divide each growing season to form a new layer of bark to the outside and a new growth ring of wood to the inside of the tree.

Wood species, the structure of wood and the location and amount of water in wood influence its drying characteristics. Sapwood contains both living and dead tissue and carries sap from the roots to the leaves. Heartwood is formed by a gradual change in the sapwood and is inactive. Generally the sapwood contains much more moisture than the heartwood, but it is more difficult to withdraw water from the heartwood because of its high resistance to fluid.

1.4 Contributions of the research work

The purpose of the research work is to study the influence of the geometrical parameters on the velocity distribution in the kiln, such as the plenum width, roof angle and sticker thickness. The effects of small gaps between boards and board irregularities because of dimensional control are also investigated. One transport wood drying model is investigated numerically. Meanwhile, the airflow and wood drying models are coupled to provide a complete calculation. The results can be used to improve drying kiln design and schedules for better product quality and energy efficiency.

Chapter 2 Airflow Modelling

2.1 Importance of airflow in the woodkiln

A schematic diagram of a woodkiln has been shown in Figure 1.1. A woodkiln provides control over the temperature, humidity, and air circulation to reduce water inside the wood to a desired value in the least amount of time, while avoiding the creation of wood defects which occur during rapid drying. Kiln operators must increase profitability of the operation by balancing the costs of improving the process versus costs associated with the loss of grade. They must try to achieve uniform drying both within a load and within a lumber piece. The uniformity of drying in wood kilns is governed, in part, by the uniformity of airflow especially in the first and second stages of drying where air convection governs the removal of the water within the wood. Uniform airflow in a kiln is influenced by such parameters as the geometry of the kiln plenum, air ducts, roof design, proper stacking of each wood package, and lumber dimensional control. All these factors can cause airflow variations which translate to different drying rates in a kiln. Minimization of airflow variations requires a thorough understanding of the mechanisms that contribute to airflow non-uniformities. Kiln operators can control airflow by regulating the fan speed, changing the fan reversal schedule, properly stacking each load, adding airflow devices, such as baffles and door strips, to minimize leakage, and enforcing lumber dimensional stability.

In recent years, there has been a trend to use a higher than normal temperature (above 100°C) to dry softwood lumber in order to reduce the total drying time. Under these conditions the external convection is relatively more important than traditional low

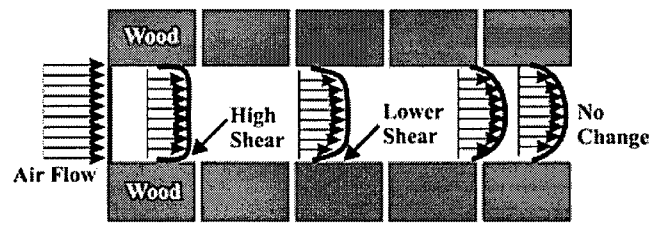
temperature drying in determining the drying time. During the removal of free water, the external heat and mass transfer will control the drying. Thus, it is important to study the airflow.

2.2 Factors that affect airflow

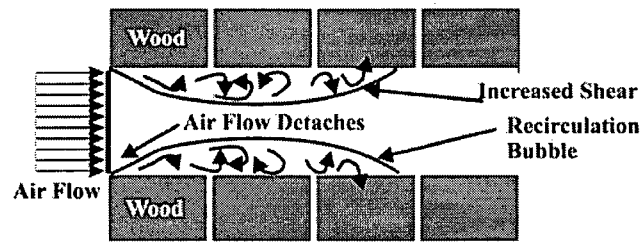
A review of possible mechanisms that can lead to airflow variations inside a kiln is discussed below.

Air Leakage: Airflow variations in kilns may be attributed to leakage if baffles are either missing or not installed, or if improper stacking of the wood creates unwanted air space. Minimizing leakage is important because air flows towards the path of least resistance to minimize pressure loss. Leakage will therefore cause more air to flow locally at one location resulting in airflow and drying variations.

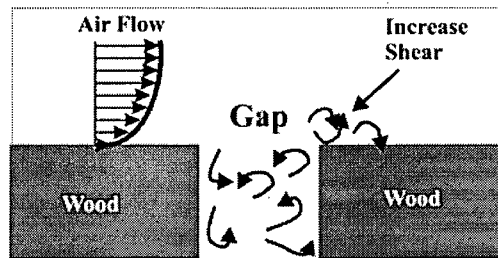
Developing Flow: Air flowing in the channels between rows of lumber forms a velocity profile, as shown in Figure 2.1a. The air sticks to the wall, thus slowing down the flow at the wall and creating a velocity gradient. The velocity gradient changes shape along the channel. When the velocity profile remains constant the flow is said to be fully developed. The mass transfer rate may double in the region where the flow is developing [22,23], because the shear stress at the wall is larger in the developing flow region. Non-uniformity in drying caused by the developing flow is reduced by reversing the flow periodically.



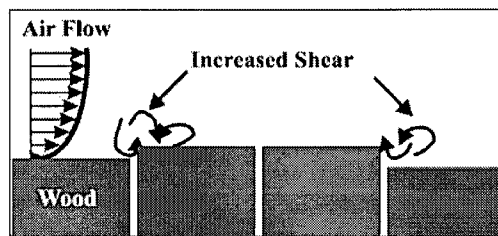
(a) Developing Flow



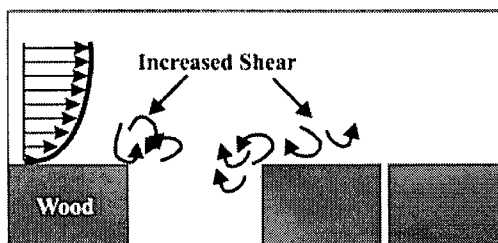
(b) Detaching Flow



(c) Small Board Gaps



(d) Board Irregularities



(e) Board Missing

Figure 2.1: Sources of Airflow Variations

Although the literature suggests sticker thickness should be large enough so as not to have fully developed flow within the stack [60], many other parameters influence the drying rate and effective drying is possible, even when the flow is fully developed within the channel.

Detaching Flow: As the air enters the channel, the airflow may detach at the leading edge due to the abrupt corner causing the flow to shear near the wall (Figure 2.1b). This separation causes flow non-uniformities near the leading edge. Non-uniformity in drying caused by the flow detaching can be reduced by reversing the flow periodically.

Small Board Gaps: The small gaps between each board have been shown to create a large local increase in the mass transfer rate near the leading edge of the boards because of the increase shear occurring as the air flows over the gap [21] (see Figure 2.1c). This increase has been predicted by flow simulation and has been measured experimentally [23,21]. A transient flow is observed in the gap accompanied by vortex shedding having a frequency varying between 1 to 7 s. Mass transfer increases of 17% to 32% for 1 to 5 mm gaps have been recorded, with the influence felt 20 to 40 mm downstream [23]. The gaps may cause airflow variations if the gaps are not approximately equal or evenly distributed throughout the load.

Board Irregularities: Unevenness in lumber height because of lack of dimensional control leads to additional shear upstream and downstream of the variation, as shown in Figure 2.1d. An increase of up to 100% in the mass transfer rate has been reported [21]. These irregularities cause airflow variations within the kiln. It has been reported that board irregularity increases the local mass transfer more than the effect caused by the gaps between boards in kiln [21].

Missing Lumber Board: When a board is missing within a package, local increase in the mass transfer coefficients occurs because of the disruption in the flow (see Figure 2.1e). An increase of up to 40% in mass transfer rates has been measured experimentally with larger increases occurring at lower velocities [49].

Uneven Sides of Packages: The sides of the packages should be even from top to bottom. This gives all sticker slots equal opportunity for airflow. When courses are staggered more than 3 inches within the package, some sticker openings get more airflow than others, as illustrated in Figure 2.2.

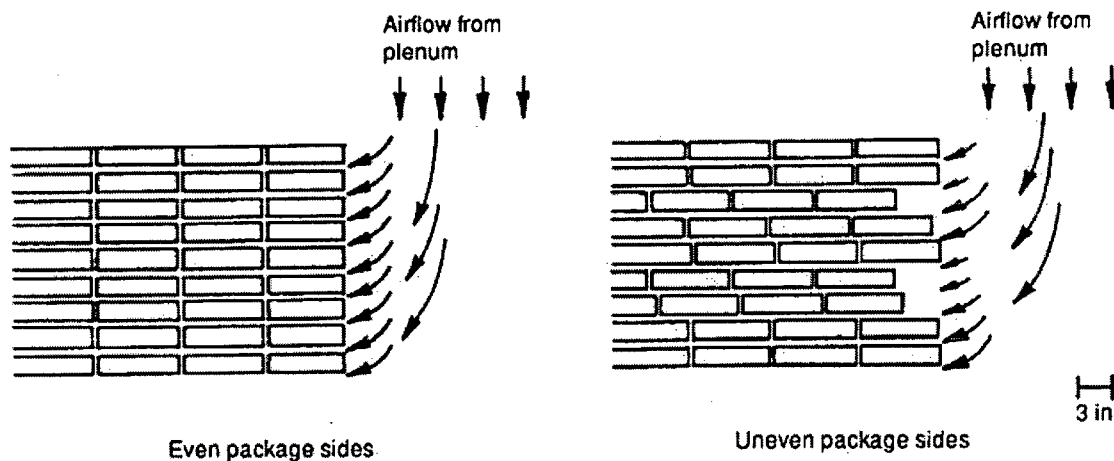


Figure 2.2: Effect of Package Unevenness

Turbulence Levels: Inlet turbulence levels are related to the velocity fluctuations in the mean flow and affect the mass transfer significantly in the kiln. Turbulence levels measured in kilns are reported to be as high as 10%. Increasing the turbulence level of the airflow from less than 1% to 8% increases the mass transfer rate by 55% for a flat plate [54]. Most mass transfer correlations are for levels of turbulence lower than those occurring in wood kilns. Measurements show that the turbulence intensity may decrease inside wood packages.

Kiln Geometry: The geometry of the kiln affects the flow distribution inside the packages. Reference [2] has investigated geometrical ratios in kilns. They conclude that the plenum width to the roof height ratio should be greater than unity. The authors also report other findings of acceptable ratios for the packages, sticker thickness, and the plenum width. Sticker thickness traditionally varies between 1/2" to 1 1/4". There is limited information on the design of kilns based on airflow considerations.

In this paper, only gaps between adjacent boards and variations in board height were investigated. One case is given for the airflow inside a typical wood kiln. Other factors, such as the effect of sticker thickness, plenum design and roof design, can be found in Reference [18].

2.3 Airflow inside a typical woodkiln

The domain of interest is divided into different flow regions, which are called computational blocks. For this study, the kiln is divided into the roof area, the plenum, and the flow channels between the wood. A solution is obtained by repeatedly applying an iterative equation solver to all the computational blocks, and cycling through all the blocks until the residuals are sufficiently small. Efficient communication between the blocks is established to achieve fast convergence by appropriately transferring data between adjacent blocks for each iteration. Detailed formulation can be found in Reference [59,17].

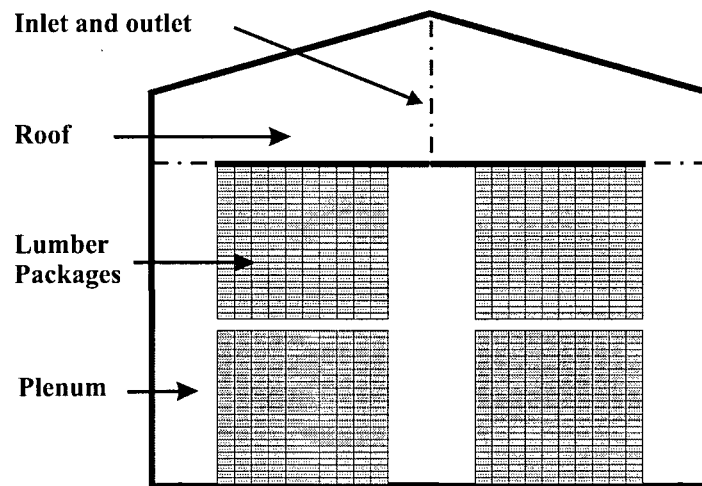


Figure 2.3: Simulated Kiln Geometry

The simulated kiln geometry is shown in Figure 2.3. The inlet velocity is 6 m/s (1082 ft/min) and the sticker thickness is 19 mm (3/4"). Two packages with 30 rows of lumber in each and separated by a 100 mm (4") gap are modeled. Rough walls, turbulent flow, no leakage, and ideal packaging are assumed. Only the slanted roof case is included in the present study. Detailed discussion of the roof design, effects of stick thickness and plenum design can be found in Reference [18]. The mesh is shown in Figure 2.4.

Figure 2.5a shows the velocity distribution inside the kiln. The "u" (horizontal) and "v" (vertical direction) velocity contours are also shown (Figure 2.5b and 2.5c). Uneven flow distribution is shown by the "u" velocity gradient in the two wood packages. The airflow increases in the gap between the packages because of the reduced flow resistance. The "v" component of the airflow reaches a maximum in the upper plenum region and gradually decreases as it approaches the bottom of the plenum.

The slanted roof causes the flow to accelerate before entering the plenum, thus causing less flow in the top channels as the downward velocity is increased at the top of the plenum. Figure 2.5d shows a recirculation bubble occurring downstream of the corner

formed by the fan deck and the upper baffle. This recirculation causes a decrease in the local pressure and a significant component in the upward airflow, thus making it more difficult for the air to enter the top channels.

The effect of airflow on the lumber drying will be discussed again in Chapter 4.4.

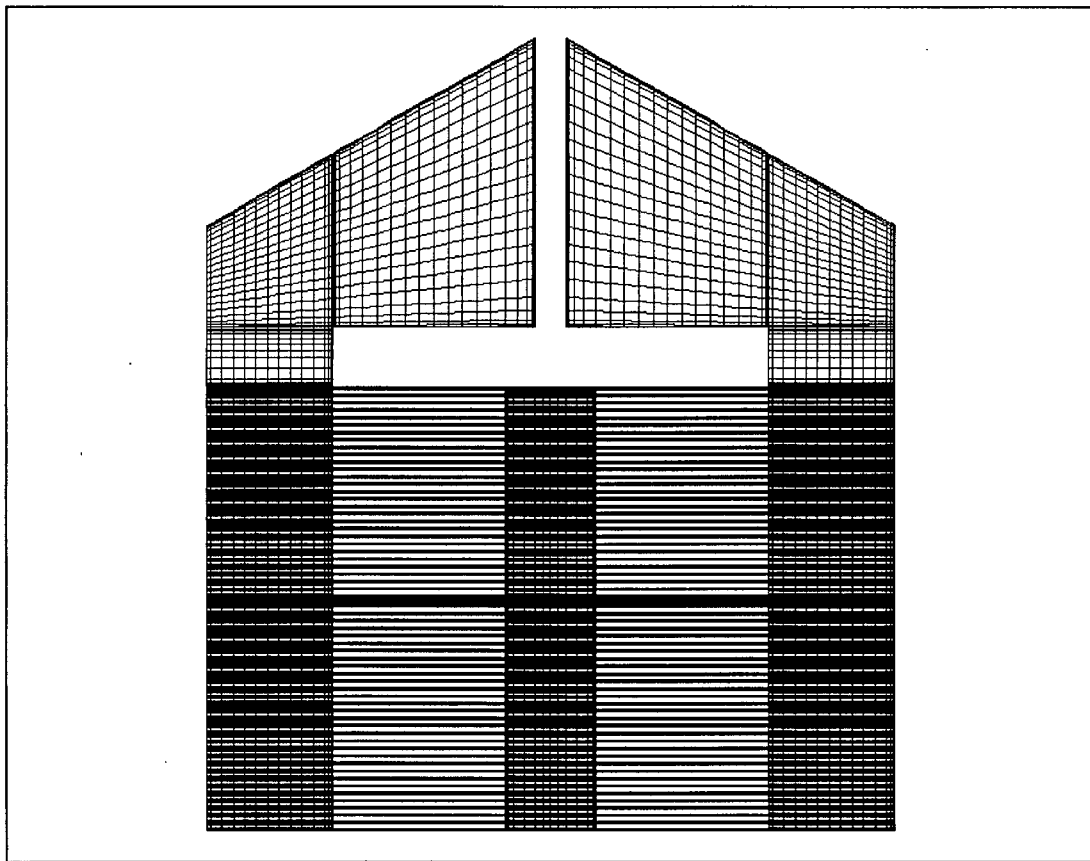


Figure 2.4: Computational Mesh for 30° Roof

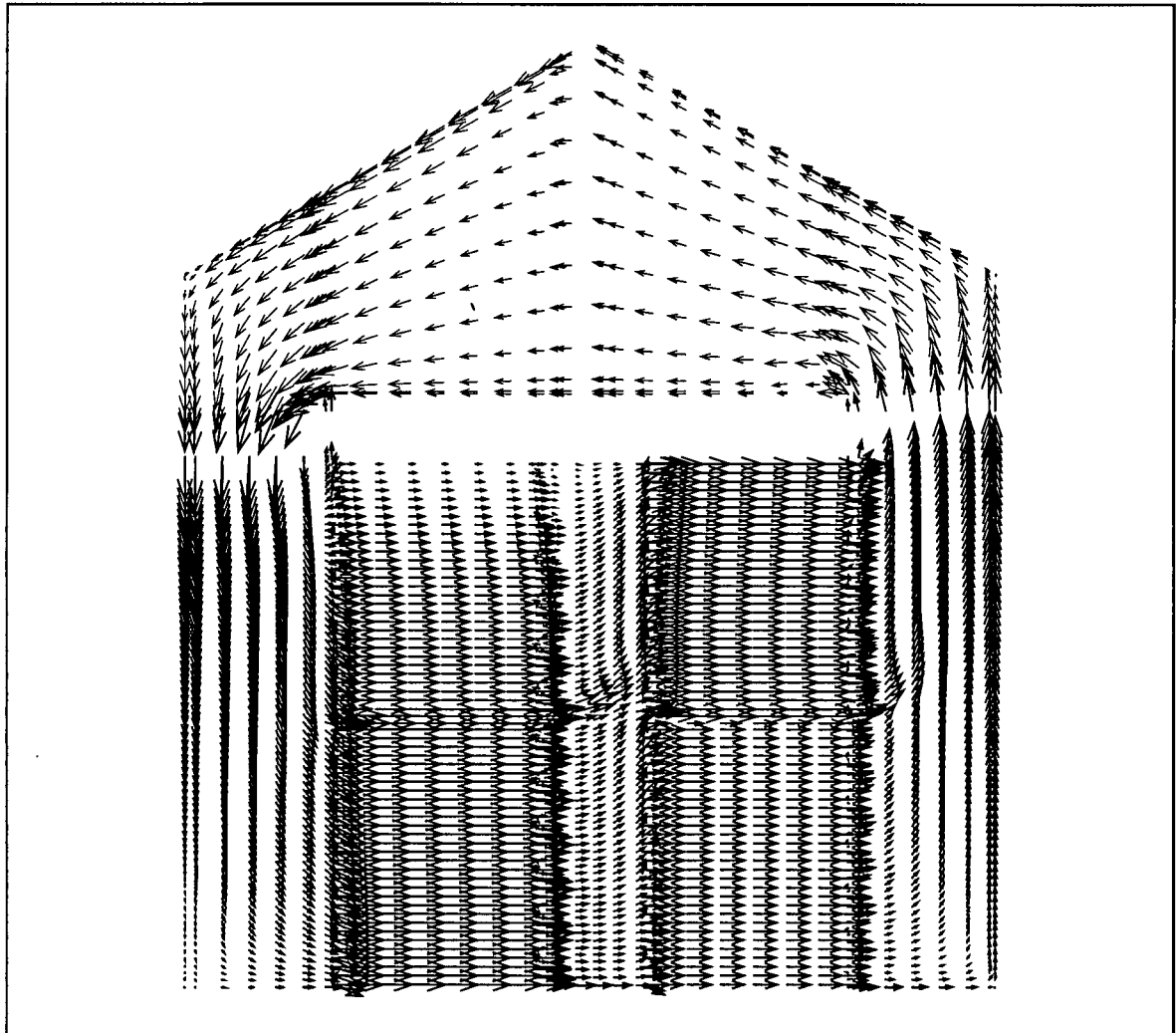


Figure 2.5a: Airflow in a typical woodkiln

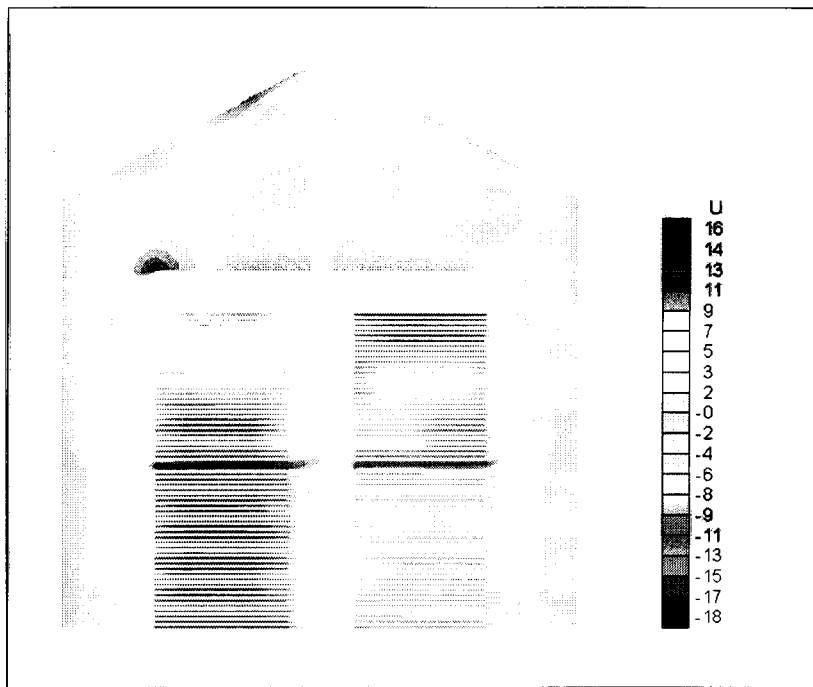


Figure 2.5b: Contour Plot of "U"

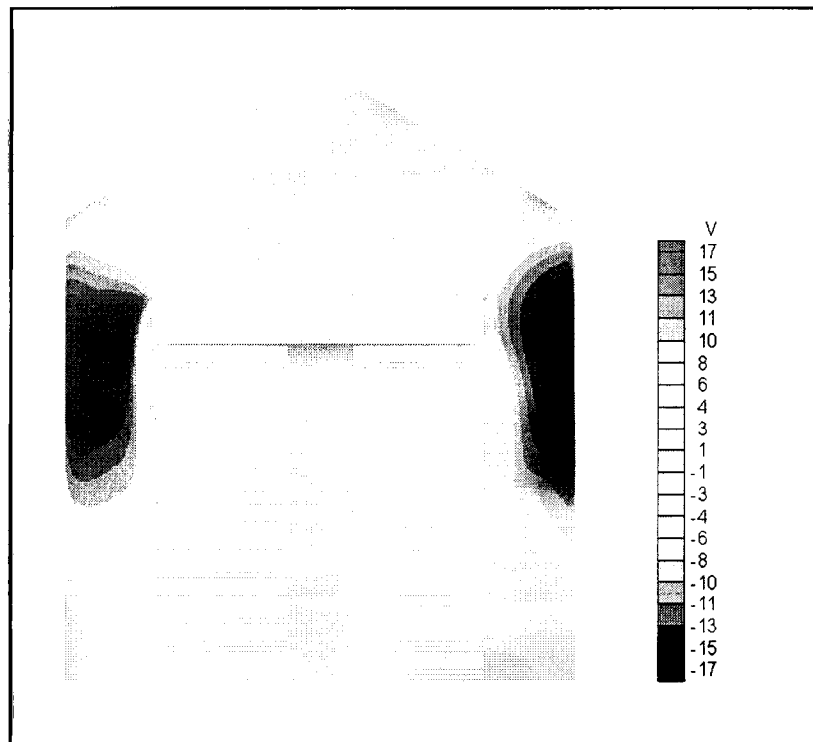


Figure 2.5c: Contour Plot of "V"

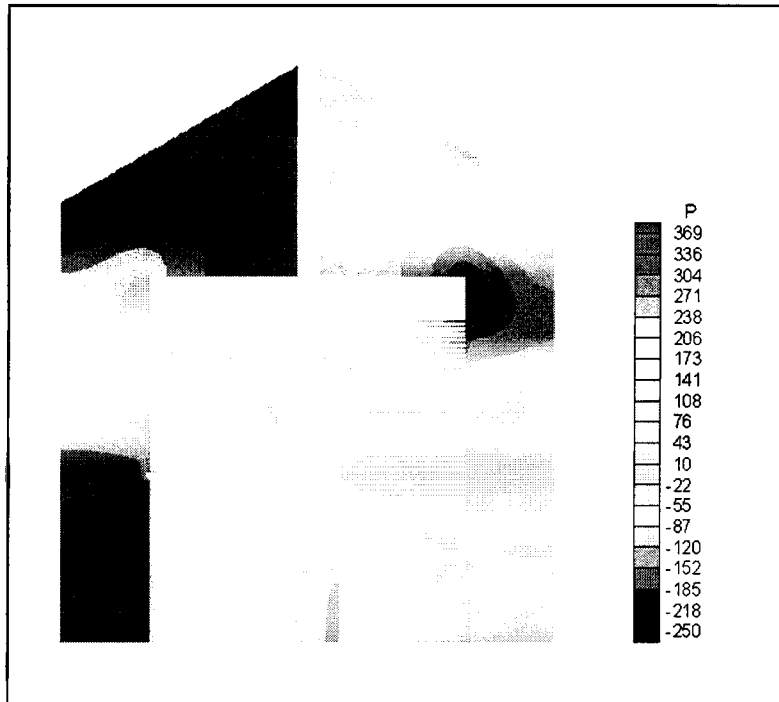


Figure 2.5d: Contour Plot of the Pressure

It was suggested that the airflow pattern as being shown in Figure 2.6 might result in a more uniform airflow distribution [11]. The reason is simple: the packages at both sides will be subjected to the airflow with similar relative humidity even without fan reverse. This case is not included in the current calculation but might be done later.

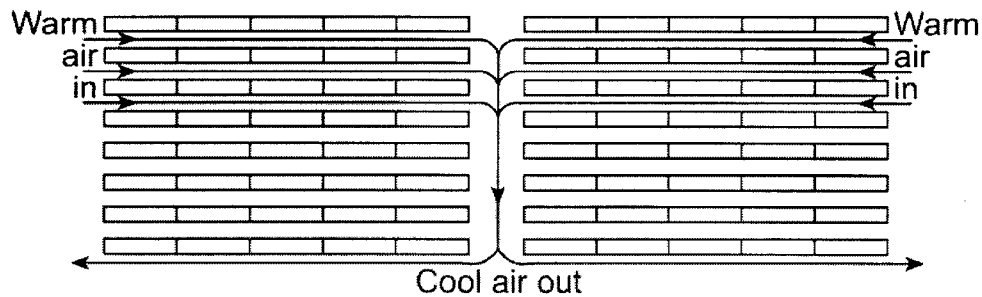


Figure 2.6: A Proposed Airflow Distribution

2.4 Modelling of the gaps and board irregularities

The effect of small board gaps and irregularities on the airflow was also simulated using a simplified geometry.

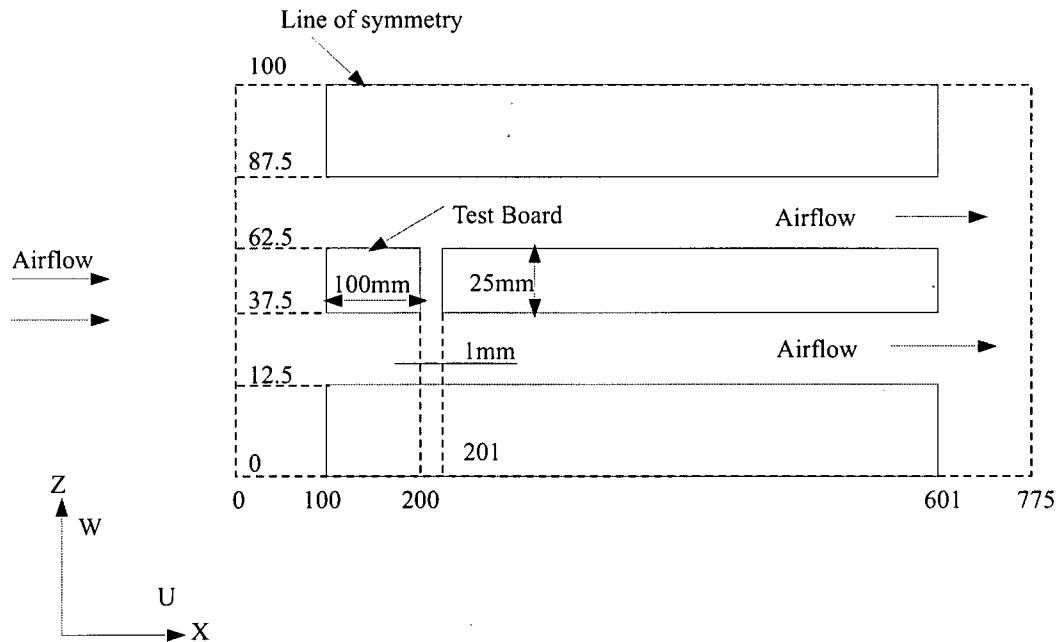


Figure 2.7: Layout of a typical flow situation

Basic Geometry: The simulated flow situation is shown in Figure 2.7. The inlet velocity is 7 m/s . In the central row, boards of $100 \times 25 \text{ mm}$ are put beside each other with side gaps of 2 mm . The gap width and board height can easily be altered to investigate different configurations. The distance between two rows of boards is the same as board thickness (25 mm). This case was previously investigated by Langrish *et al* [22] numerically, but it was reported that the results were not satisfactory.

The heat and mass transfer processes at the surface of the boards are of great importance, therefore refined grids near the wall, as well as the leading and trailing edge

corners, were used to obtain a more accurate solution. A typical grid is shown in Figure 2.8.

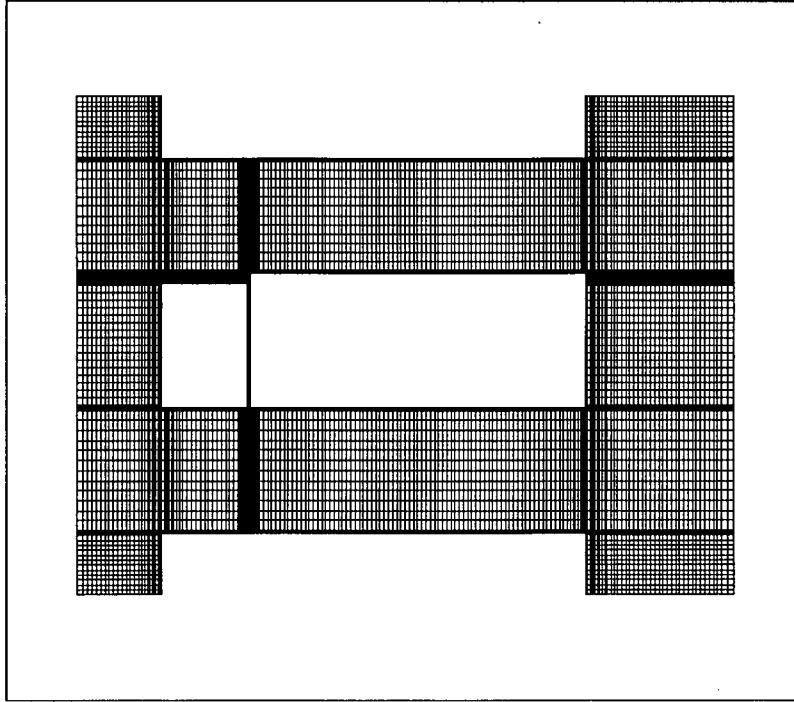


Figure 2.8: Grid layout of the simulation

In the simulation, the wall shear stress is calculated from the following equation:

$$\tau_w = \rho C_\mu^{1/2} K_p \quad (2.1)$$

The Colburn analogy between mass and momentum transfer is used to related the wall shear stresses to the heat and mass transfer coefficients, therefore for mass transfer:

$$\frac{Sh_x}{Re_x Sc} \cdot Sc^{2/3} = \frac{C_f}{2}$$

$$C_f = \frac{\tau_w}{\rho u^2 / 2} \quad (2.2)$$

where:

$Sc = v/D_{AB}$ is the Schmidt number;

$Sh_x = k_x x / D_{AB}$ is the local Sherwood number;

k is the local mass transfer coefficient (m/s);

ν is the kinetic viscosity of air (m²/s);

x is the distance from the leading edge of the lumber (m);

u is the bulk velocity above the lumber (m/s);

D_{AB} is the diffusivity of the water vapor through air (m²/s).

C_f is the skin-friction coefficient.

For heat transfer, we can use the Reynolds analogy:

$$St \cdot Pr^{2/3} = \frac{1}{2} C_f$$

$$St = \frac{Nu_x}{Re_x Pr} \quad (2.3)$$

Where:

St is the Stanton Number

$Nu_x = \frac{h_m x}{k}$ is the Nusselt number;

$Pr = \frac{\mu C_p}{k}$ is the Prandtl number.

Gaps between Boards: Figure 2.9 shows the variations of the shear stress with distance as predicted by the numerical simulation. The result described the trend in the shear stress, but the magnitude of the enhancement is less than that of the literature work. Various board side gaps were investigated. The result shows that large gaps (5mm or larger) enhanced the local shear stress more than that of small gaps (2mm).

Board Irregularities: In order to investigate the effect of the irregularities in the board height due to sawing and shrinkage, the second board was considered to be higher than the first one. The third board was put lower than the second one in order to compare the effects of height irregularities on the leading and trailing edges of the variations. Figure 2.10 shows the velocity distribution in the flow field. It can be seen that the flow pattern is significantly altered near the leading and trailing edges of the variations.

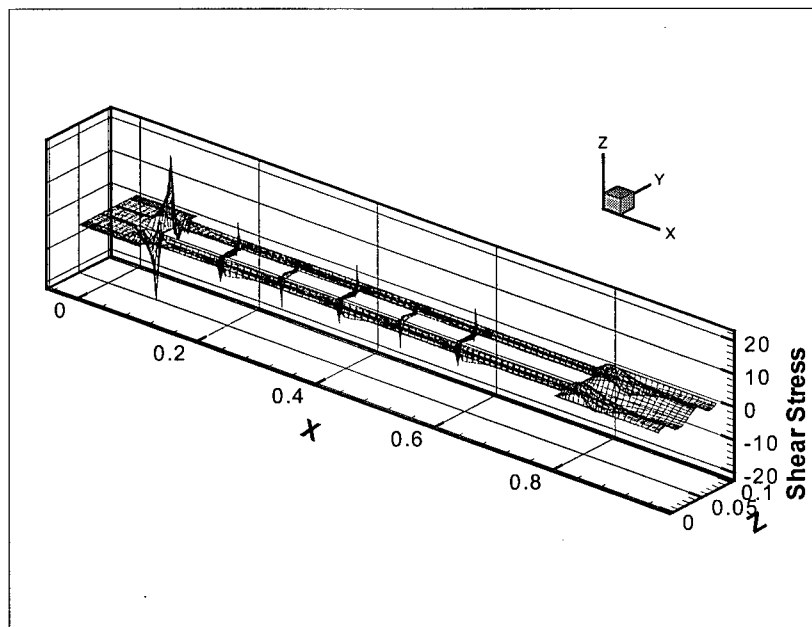


Figure 2.9: Shear stress distribution

Both a thinner leading and a thinner trailing board in the direction of the airflow can dramatically change the flow near the variation areas and increase the local shear thus the heat and mass transfer coefficient (Figure 2.9). The actual values depend on the velocity, the height difference, etc. An increase in variation in the height of the adjacent boards on either side of the board will raise the local mass transfer coefficient. A thinner leading board increased the shear stress more than that of a thinner trailing board.

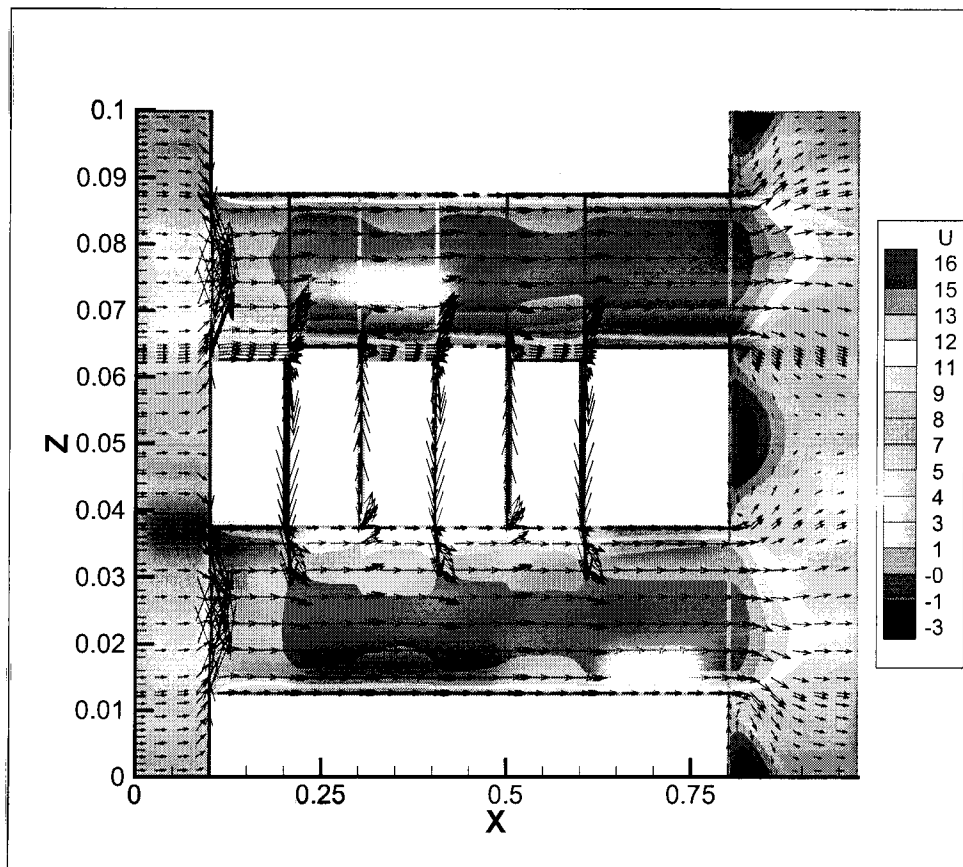


Figure 2.10: Velocity Distribution

Figures 2.8 to 2.10 also show that the effect of the board height variations on the local heat and mass transfer coefficient is more significant than that of the gaps between the boards.

The results imply that both the gaps and board irregularities might reduce the drying time for the lumber pieces at normal thickness during the first stage of the drying when the free water is present. However, it will also take longer to dry the lumber pieces at higher than normal thickness, thus lead to non-uniformity in drying. In addition, gaps will reduce the volume of lumber which can be dried in the kiln. Therefore, proper methods, such as fan reversal, have to be introduced to prevent this kind of non-uniformity.

Chapter 3 Wood Drying Modelling

3.1 Overview of the Various Wood Drying Models

The transport of fluids through wood can be divided into two main types. The first is the bulk flow of fluids through the interconnected voids of the wood under the driving of a pressure gradient. The second is diffusion which can be subdivided into two types: intergas diffusion, which includes the transport of water vapor through the air inside the wood, and bound water diffusion within the cell walls. The magnitude of the bulk flow of a fluid through wood is determined by its permeability, which is a measure of the ease with which fluids are transported through a porous solid under the influence of a pressure gradient.

During the past 20 years a large effort has been undertaken to understand the water movement in wood during drying; as a result, numerous wood drying models have been developed. In general, these models can be classified in three categories: (1) diffusion models; (2) empirical curve-fitting models; (3) transport wood drying models [42]. The diffusion models are a special case of transport wood drying models. Empirical models lack the prediction capability when the drying conditions fall outside the range of conditions from which they were derived [42]. Transport wood drying models are the most frequently used models. They are of two types: (1) models based on a potential term (Luikov 1966) [25], and (2) multi-component models (Whitaker 1977) [57,58].

Following Luikov's (1966) approach, Fortin *et al.* [8] used the water potential concept to characterize water movement in wood in terms of energy. A model of isothermal wood

drying using the gradient in water potential as the drying force was developed. This will be introduced in Chapter 3.2.

The multi-component approach was proposed by Whitaker(1977). Conservation relations are written for liquid water, water vapor, and the gaseous mixture (water vapor + air). An energy balance equation is also written considering the contribution of each component of the system. The multi-component interactions described at the microscopic level are averaged over a representative control volume. A set of macroscopic equations is then obtained by which the fluxes of the different components are described using different transport coefficients and driving forces. The gradient in the total pressure of the gaseous phase is considered to be the driving force of the gas mixture, and the gradient in pressure within the liquid is considered to be the driving force of the liquid state (according to Darcy's law). The flux of water vapor is obtained by taking the vapor component of the gas mixture flux plus a term describing the diffusion of water vapor driven by the gradient in vapor concentration. This approach has been applied to wood by several authors as shown in Table 3.1.

Table 3.1: Different Wood Drying Models.

Authors	Parameters	Dimension	Basis & Type
P. Perre (1991~1994) [33,34,36,37,38]	3 Eqns. (M,T,P)	2D	Whitaker's theory. Transport Wood Drying Models.
A. Cloutier (1991~1994) [7,8,9]	1 Eqn. (M) Requiring M- ψ and K- ψ Relationship	2D	Water-Potential Concept. Transport Wood Drying Models.
O. A. Plumb (1994) [39]	2 Eqns. (M,T)	2D	Whitaker's theory.
I. W. Turner (1994~1995) [56]	3 Eqns. (M,T,P)	2D	Self-contained. Transport Models.

3.2 Wood Drying model based on water-potential

The water potential concept can theoretically be applied to both bound water and free water. The gradient in water potential can therefore be used as the driving force within the whole range of moisture contents provided the moisture content-water potential relationship ($M-\psi$) is known. Fortin (1979) evaluated the boundary desorption and absorption curves of the $M-\psi$ relationship of western hemlock at high moisture contents. Variations in the shape of the $M-\psi$ relationship at high moisture contents within or between species can be explained on the basis of anatomical differences, since water potential takes capillary forces into account. Temperature can also have a significant effect on the $M-\psi$ relationship at high moisture contents.

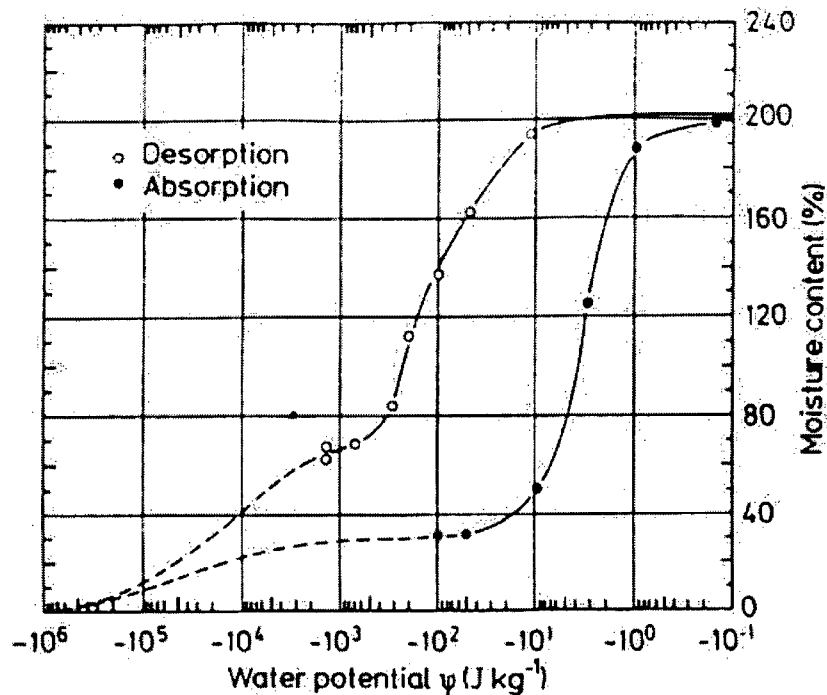


Figure 3.1: Moisture content-water potential relationship of western hemlock sapwood along the boundary desorption and absorption curves at 21 °C (From A. Cloutier 1991)

The water potential is defined as:

$$\psi = \bar{G} - \bar{G}_0 \quad (3.1)$$

where \bar{G} = specific Gibbs free energy of water in the state under consideration; \bar{G}_0 = specific Gibbs free energy of water in standard reference state.

The concept of water potential is derived from the combination of the first and second laws of classical thermodynamics with the Gibbs free energy function. The wood-water-air system is regarded as a three-phase system, of which only the phase "water" is considered. Since the water movement in wood during drying is quite slow, this system can be considered to be a closed system in thermodynamic equilibrium with its surroundings.

The governing equation is: $\frac{\partial M}{\partial t} + \frac{\partial}{\partial X}(D_x \frac{\partial M}{\partial X}) + \frac{\partial}{\partial Y}(D_y \frac{\partial M}{\partial Y}) = 0$, where M is the moisture content, D_x and D_y are coefficients which can be regarded as a functions of $\frac{\partial \psi}{\partial M}$. Therefore M can easily be found out if the ψ -M relationship is known. A detailed derivation of the equation can be found elsewhere [7,8,9].

The wood drying model based on the water potential concept is a relatively new one. It is claimed that a potential function should be used as the driving force since its space derivative gives a force and thus corresponds to a real driving force. This depends on the experiment, since the water potential-moisture content (M- ψ) and effective water conductivity-moisture content (K- ψ) relationship have to be experimentally determined. At present, it can only deal with isothermal and isobaric cases. If the M- ψ and K- ψ

relationship are available at various temperatures, it will be a good model, since only one equation is needed.

3.3 Mathematical Model

In the present work a wood drying model based on simultaneous heat and mass transfer as developed by Perre and Morne [33,34,36,37,38] is described. Related models are listed in Table 3.1.

We consider a rigid porous medium, which contains three phases: solid(s), liquid(L), gas(g). The gas phase has two components: water vapor (v) and air (a). The following major assumptions are made in developing the model and the computational code:

1. Both the solid and gas phases are continuous, as is the liquid phase in the wet region.
Both liquid and gas phase motion are slow so that convective accelerations can be ignored.
2. The binary gas mixture of air and vapor behaves like an ideal gas.
3. Darcy's law holds for the gas and free liquid phases. Gravity is important for the liquid but not for the gas phase.
4. The differential heat of sorption (specific heat of wood as a function of moisture content) is included for the treatment of the enthalpy of bound water. Suppose the energy required to evaporate water from the cell wall of wood is Q_1 , and the energy required to evaporate water from the liquid state is Q_2 , then the difference $Q_1 - Q_2$ is the differential heat of sorption.

5. The medium is assumed to be in thermodynamic equilibrium: the temperatures in the three phases are the same; the vapor pressure in the gas is given by its equilibrium value.
6. The phase kinetic energies, the fluid viscous dissipation and the work done by the body forces are negligible.

Other assumptions are also listed here. The thermal conductivity of each phase is constant. Latent heat of vaporization is constant. The enthalpy in the three phases is a linear function of temperature. The cell wall material is assumed to be rigid above FSP with constant density.

3.3.1 Equations governing timber drying

The governing equations are written as follows:

Mass balance

The macroscopic mass balance for the liquid phase is written as:

$$\rho_o \frac{\partial M_L}{\partial t} = -\nabla \cdot \vec{n}_L - \dot{m} \quad (3.2)$$

$$\text{With } \vec{n}_L = \rho_L \vec{V}_L$$

where: M_L is the mass fraction of liquid water per unit mass of dry solid.

ρ_o is the dry solid density

ρ_L is the liquid density

\vec{n}_L is the liquid mass flux density

\vec{V}_L is the superficial liquid velocity

m is the phase change term (that is the mass of evaporated water per unit volume of porous medium and per unit time).

As the gas phase has two components, the mass balances for water vapor and air are written respectively:

Vapor:

$$\rho_o \frac{\partial M_v}{\partial t} = -\nabla \cdot \vec{n}_v + m \quad (3.3)$$

$$\text{With } \vec{n}_v = \rho_v \vec{V}_g + \vec{j}_v$$

Air:

$$\rho_o \frac{\partial M_a}{\partial t} = -\nabla \cdot \vec{n}_a \quad (3.4)$$

$$\text{With } \vec{n}_a = \rho_a \vec{V}_g + \vec{j}_a$$

where:

M_v (or M_a) is the water vapor (or air) mass fraction per unit mass of dry solid.

ρ_v (or ρ_a) is the water vapor (or air) density in the gas phase.

\vec{n}_v (or \vec{n}_a) is the water vapor (or air) mass flux density relative to a fixed frame.

\vec{V}_g is the superficial gas velocity.

$\vec{j}_v = -\vec{j}_a$ is the diffusive mass flux density of vapor diffusion relative to the mass-averaged velocity \vec{V}_g .

The superficial velocity of liquid and gaseous phase is calculated using Darcy's Law. The bound water is treated separately by using the following expression:

$$\vec{n}_L = \rho_L \vec{V}_L = -\rho_0 D_b \nabla X_L \quad (3.5)$$

Energy Balance

The energy conservation is written as follows:

$$\frac{\partial}{\partial t}(\overline{\rho h}) + \nabla \cdot (\overline{\rho u h}) = \nabla \cdot (\lambda_{eff} \nabla \overline{T}) \quad (3.6)$$

$$\text{Where } \overline{\rho h} = \rho_0 (h_s + \int_0^{X_L} h_L dX_L + X_v h_v + X_a h_a)$$

$$\overline{\rho u h} = h_s + h_L (X_L) \overline{n}_L + h_v \overline{n}_v + h_a \overline{n}_a$$

Here subscript s , L , v and a denotes solid, liquid, vapor and air, respectively, and h_i ($i = s, L, v, a$) represents the enthalpy of component i . For air, water vapor and solid wood, the enthalpy is assumed to be a function of temperature only. For liquid, it is assumed to be a function of both temperature and moisture content.

Among the several choices of three independent variables, the temperature T , the moisture M and the total pressure in the gaseous phase are retained:

$$\frac{\partial M}{\partial t} = \vec{\nabla} \cdot (D_M \vec{\nabla} M + D_T \vec{\nabla} T + D_P \vec{\nabla} P)$$

$$\rho_0 C_p \frac{\partial T}{\partial t} + \left(\frac{\partial h_L}{\partial X_L} \right)_T n_L \vec{\nabla} X_L = \vec{\nabla} (K \cdot \vec{\nabla} T + \rho_0 \Delta h_v D_M^V \vec{\nabla} M + \rho_0 \Delta h_v D_P^V \vec{\nabla} P) \quad (3.7)$$

$$\alpha \frac{\partial P}{\partial t} - \beta \frac{\partial M}{\partial t} - \gamma \frac{\partial T}{\partial t} = \vec{\nabla} (-D_T^V \vec{\nabla} T - D_M^V \vec{\nabla} M + D_P^a \vec{\nabla} P)$$

Here D_i ($i = M, T, P$) is a phenomenological coefficient which is a function of wood species and moisture content M , temperature T and pressure P , respectively. A detailed description of these coefficients is listed in the appendix.

The set of equations can be rearranged for computational convenience.

$$\begin{aligned} \frac{\partial M}{\partial t} &= \nabla \cdot (K_{11} \nabla M) + \nabla \cdot (K_{12} \nabla T) + \nabla \cdot (K_{13} \nabla P) \\ \frac{\partial T}{\partial t} &= \nabla \cdot (K_{21} \nabla M) + \nabla \cdot (K_{22} \nabla T) + \nabla \cdot (K_{23} \nabla P) + S_1 \\ \frac{\partial P}{\partial t} &= \nabla \cdot (K_{31} \nabla M) + \nabla \cdot (K_{32} \nabla T) + \nabla \cdot (K_{33} \nabla P) + S_2 \end{aligned} \quad (3.8)$$

where:

M is the moisture content based on oven-dry wood (calculated as the difference between the initial wet weight and the oven-dry weight, divided by the oven-dry weight and multiplied by 100 percent, i.e., $100 \cdot (M_{\text{Wet}} - M_{\text{Dry}}) / M_{\text{Dry}}$).

T is the temperature.

P is the total pressure in the gaseous phase.

K is the capacity coefficient, which depends on wood species.

S is the source term due to the differential heat of sorption (heat capacity of liquid phase as a function of moisture content).

3.3.2 Boundary Conditions

A drying at atmosphere pressure (P_{atm}) is considered. The total pressure in the gaseous phase is constant throughout the boundary layer. Therefore:

$$P_g = P_{\text{atm}} \quad (3.9)$$

At the exchanging surface (see Figure 3.2), the mass flux is given by:

$$\begin{aligned} \Phi_m &= (\overline{n_L} + \overline{n_v}) \cdot \overline{n} \\ &= -\rho_0 (D_x \vec{\nabla} X + D_T \vec{\nabla} T + D_P \vec{\nabla} P_g) \cdot \overline{n} \end{aligned} \quad (3.10)$$

The left-hand side of the equation denotes the mass flux density at the interface (water that goes into the airflow). The three terms on the right-hand side of the equation represent the mass flux caused by the gradient of moisture content, temperature and pressure, respectively.

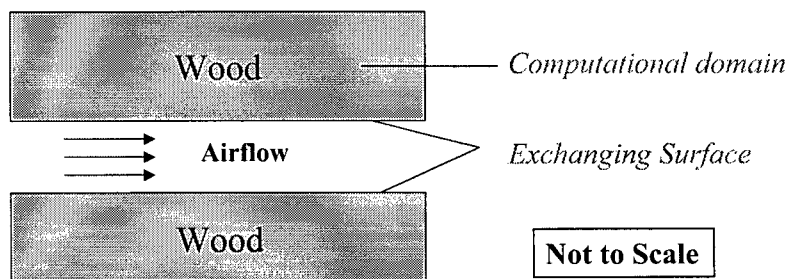


Figure 3.2: Boundary Condition

The heat flux at the exchanging surface is given by:

$$-(k\vec{\nabla}T + \rho_0\Delta h_v D_x^v \vec{\nabla}X + \rho_0\Delta h_v D_p^v \vec{\nabla}P_g) \cdot \vec{n} + \Phi_h - \Delta h_v \Phi_m = 0 \quad (3.11)$$

Here the first three terms represent the flux due to the gradients of temperature, moisture content and total pressure of the gaseous phase, respectively; Φ_h is the heat flux density at the interface (from the airflow); the last term is related to the phase change term and the differential heat of sorption.

The convective heat and mass flux from the airflow is calculated using the following expression:

$$\begin{aligned} \Phi_m &= h_m \times (\rho_w - \rho_\infty) \\ \Phi_h &= h \times (T_\infty - T_w) \end{aligned} \quad (3.12)$$

Here h and h_m are heat and mass transfer coefficients calculated using Reynolds analogy and Colburn analogy.

3.3.3 Sub-model used in the simulation

The wood drying model proposed by S. Pang [30,31,32] is also used in the calculation. This is a two-parameter model. It is postulated for the drying of heartwood that liquid flow does not occur within the wood due to the aspirated state of the pits, so an evaporative plane at the boiling point of water sweeps through the timber until the center of the board is reached. In the case of the much wetter sapwood where the pits are not initially aspirated, it is assumed that liquid flow initially maintains an evaporative plane just below the surface until the moisture is no longer funicular. Thereafter, drying proceeds in a similar way to heartwood.

The evaporative plane divides the material into two parts, a wet zone beneath the plane and a dry zone above it. This can be shown in the following figure. Detailed models of heartwood and sapwood both use this concept as described below.

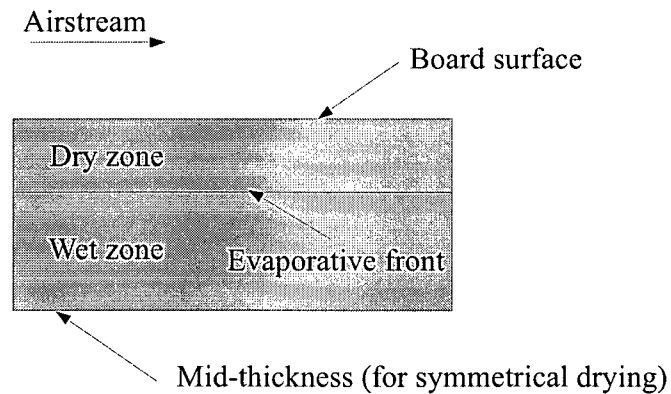


Figure 3.3: The evaporative front model for drying of a softwood board.

Heartwood

Since the pits in the heartwood are already aspirated, it is postulated that at the evaporative plane all the free water evaporates, and that this plane recedes into the material as drying proceeds. Above the plane, water is assumed to exist as bound water and water vapor. Bound water will be in local thermodynamic equilibrium with the vapor pressure of water at the local temperature. In the wet zone, the moisture content remains at the initial value. After the evaporative plane reaches the center-layer of the board, drying is controlled by bound water diffusion and water vapor flow.

Sapwood

In sapwood, there should be little flow of liquid moisture close to the surface, since most of the pits near the surface are aspirated during sawing. Therefore, at the beginning of the initial drying period for sapwood, the evaporative plane should recede into the

material very quickly until it reaches a distance ξ . However, for places located at distances larger than the distance “ ξ ” from the surface, most of the pits inside this position are not yet aspirated, while the flow of liquid is no longer negligible as the lumens are almost completely saturated. The liquid flow toward the surface keeps the evaporative plane at the position ξ until the moisture content at the plane decreases to the minimum value for liquid continuity. After this, the plane will start to recede into the material.

Mixed wood

The behavior of mixed wood is assumed to be intermediate between that of heart- and sapwood. Appropriate adjustment of the transport parameters and the "mean" recession of the thin drying layer has to be made.

3.3.4 Equilibrium Moisture Content

Liquid water in wood exists in two basic forms: bound water within the cell wall and free water in the voids of the wood. An equilibrium is obtained between the bound water and the relative humidity of the surrounding airflow. A relative humidity of 0% corresponds to a zero wood moisture content. This equilibrium moisture content gradually increases with the relative humidity until the cell wall becomes saturated when the relative humidity reaches 100%. This point is called fibre saturation point.

When the moisture content of the exchanging surface drops below FSP (Fibre Saturation Point), the EMC (Equilibrium Moisture Content) is used. FSP is defined as the moisture content at which the cell walls are saturated with bound water but no free water exists in the cell cavities. EMC is defined as the moisture content of wood which has

been exposed to the same conditions of temperature and humidity for a sufficiently long period to reach equilibrium [26]. Under constant external conditions, wood will continue to dry until an equilibrium moisture content, X_c , is reached below the FSP. The value of X_c depends on dry-bulb temperature and humidity, which can be expressed in terms of a wet-bulb temperature or wet-bulb depression.

The following model can predict EMC within 1% MC [44,47]. The model is:

$$M = \left[\frac{K_1 K_2 RH}{1 + K_1 K_2 RH} + \frac{K_2 RH}{1 - K_2 RH} \right] \frac{18}{K_3} \quad (3.13)$$

where

$$K_1 = 4.737 + 4.774 \times 10^{-2} T - 5.012 \times 10^{-4} T^2$$

$$K_2 = 0.7059 + 1.697 \times 10^{-3} T - 5.553 \times 10^{-6} T^2$$

$$K_3 = 223.4 + 0.694 T + 0.01853 T^2$$

T is the dry-bulb temperature, and RH is the relative humidity of the airflow.

Although relative humidity and temperature are the most important factors affecting EMC, other factors, such as mechanical stress, drying history of the wood, species and specific gravity of the wood, also influence EMC. In general, an increase in compressive stress decreases EMC. In addition, the EMC is higher during desorption than during adsorption. These factors are not included in the model.

3.4 Results and Discussions

We have investigated the drying process of a single spruce piece under different external conditions (different airflow at certain locations of the kiln as shown in Figure 3.4). In this study, the four sides (left, right, bottom and top) were assumed to be subjected to the same airflow condition, i.e., same dry-bulb, wet-bulb temperature and heat and mass transfer coefficients.

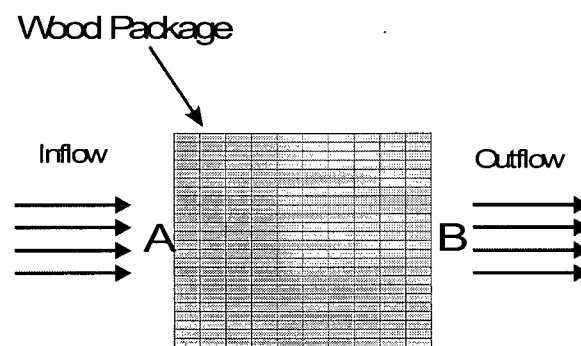


Figure 3.4: Locations of the selected wood pieces
The parameters for the different cases are listed here:

Length=0.2m, Height=0.05m, Initial Pressure=1 atm.

- Case1 (outlet, part B in Figure 3.4):
 $T_{db}=353\text{K}(80^{\circ}\text{C})$, $T_{wb}=333\text{K}(60^{\circ}\text{C})$,
 Initial Moisture Content=1.0,
 Initial Temperature of Lumber=293K(20°C).
- Case2 (inlet, part A in Figure 3.4):
 $T_{db}=373\text{K}(100^{\circ}\text{C})$, $T_{wb}=353\text{K}(80^{\circ}\text{C})$,
 Initial Moisture Content=1.0
 Initial Temperature of Lumber=293K(20°C).
- Case3 (High Temperature):
 $T_{db}=393\text{K}(120^{\circ}\text{C})$, $T_{wb}=353\text{K}(80^{\circ}\text{C})$,
 Initial Moisture Content=1.0

Initial Temperature of Lumber=293K(20°C).

- Case4 (Forintek 1):

T_{db} and T_{wb} are the same as the experiment.

Initial Moisture Content=0.66,

Initial Temperature of Lumber=293K(20°C).

- Case5 (Forintek 2):

T_{db} and T_{wb} are the same as the experiment.

Initial Moisture Content=0.78,

Initial Temperature of Lumber=293K(20°C).

Here T_{db} and T_{wb} are dry-bulb and wet-bulb temperatures, respectively, inside the kiln. EMC and the heat and mass transfer coefficients are calculated according to the flow variables (velocity, humidity, etc).

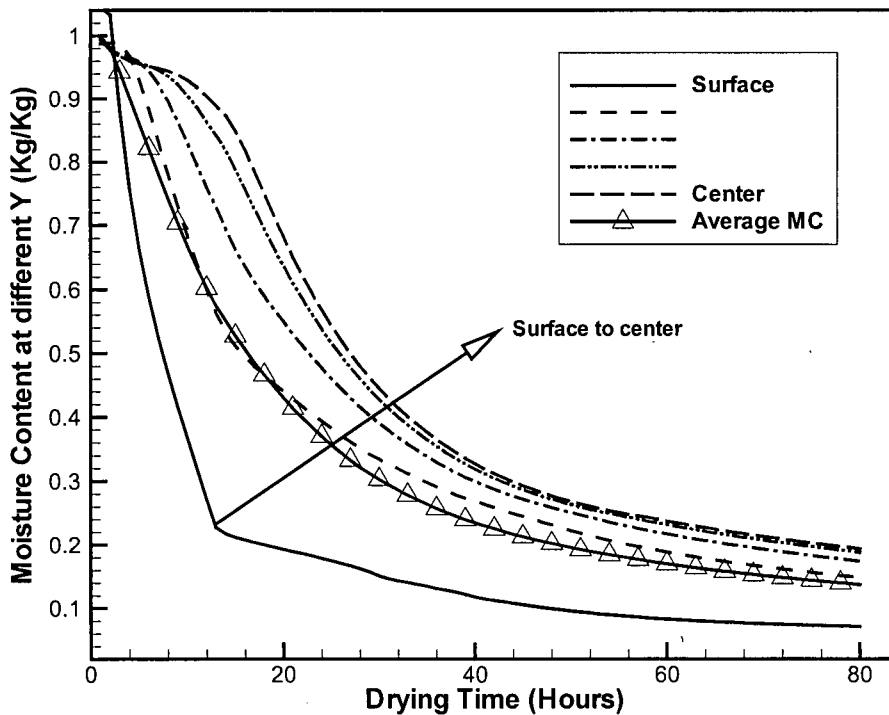


Figure 3.5: Moisture content at different Y as a function of drying time (Case 1)

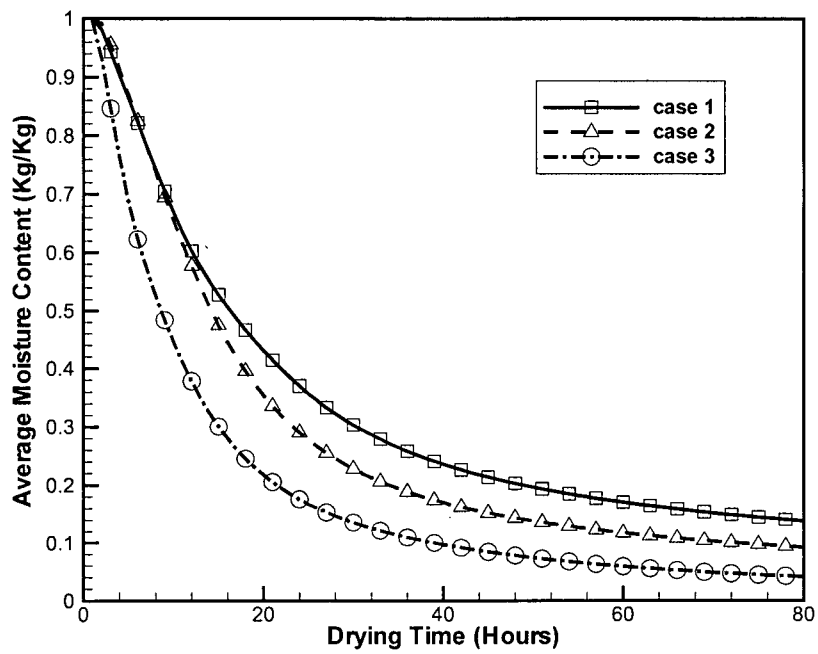


Figure 3.6: Average moisture content as a function of drying time (Case 1,2 and 3)

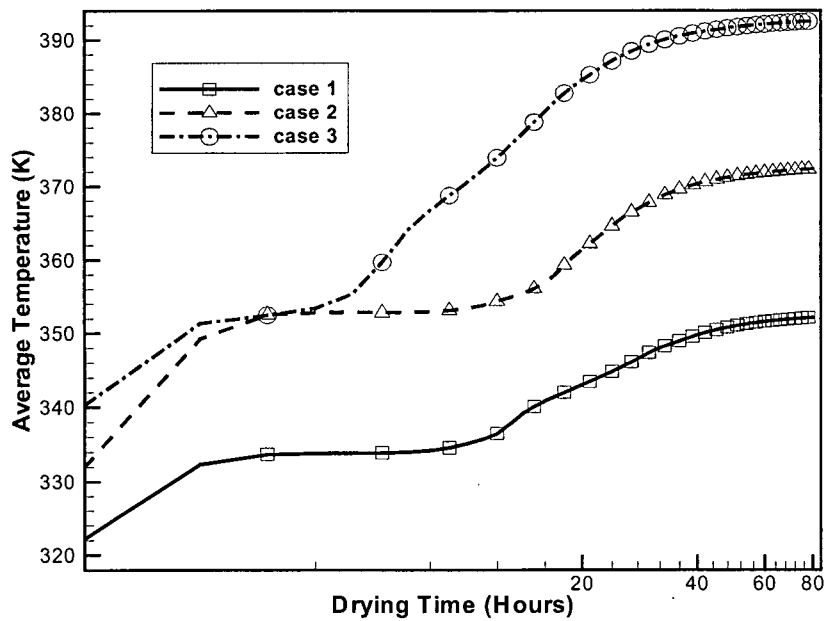


Figure 3.7: Average temperature as a function of drying time (Case 1,2 and 3)

3.4.1 Description of drying process

Figure 3.5 shows the spatial moisture content distribution (from surface to center) for case 1. It can be seen from the figures that during the first few hours, the moisture content strongly decreases near the exchange surfaces. The drying rate is high and relatively constant. As the drying progresses the drying rate decreases. When all the free water is removed, the diffusion of bound water and the convective migration of the vapor ensure the transport of mass.

Figures 3.6 and 3.7 show the average moisture content and temperature as a function of drying time for case 1, 2 and 3. In the first few hours, the temperature is below the dry bulb temperature. The temperature increases to the wet-bulb temperature. It remains constant at the wet-bulb temperature when free water is still present. This is called the constant drying rate period. When free water is not present in some part of the wood, the temperature shows a second increase.

From the plot of average moisture content for the three cases, we can see that during the constant drying rate period, the temperature need not be very high. It is convective mass transfer dominant. Keeping a suitable wet-bulb temperature depression is very important for this period, since this will affect both drying time and drying quality. When free water is not present, the temperature will become the dominant factor in drying.

One way to reduce drying cost is to use the continuously rising temperature (CRT) process. It was reported that using of CRT can reduce drying time, energy and the drying defect. During the first stage of the drying when free water is present, the temperature of the lumber surface is assumed to be at the wet-bulb temperature. As drying progresses, the surface temperature rises and approaches the dry-bulb temperature. The dry-bulb

temperature is then set to a higher value which makes the temperature difference between the air and the wood relatively constant. This will minimize drying defects.

Figures 3.8 and 3.9 show the average moisture content during the drying process of two cases compared with experimental data obtained from Forintek Canada Corporation. In the experiment, the dry and wet bulb temperature of the airflow and the weight of the wood package were measured every half hour. The dry-bulb and wet-bulb temperature in the model was fitted to the values used in the experiment. It can be seen that there is a reasonable agreement between numerical results and experiment. It can also be seen that the drying rate during the first few hours is relatively higher than in the later stage. The differences may be explained by the using of lumber piece in the model instead of the lumber package in the experiment. Further experiments may investigate the moisture content distribution in a piece of lumber instead of a wood package.

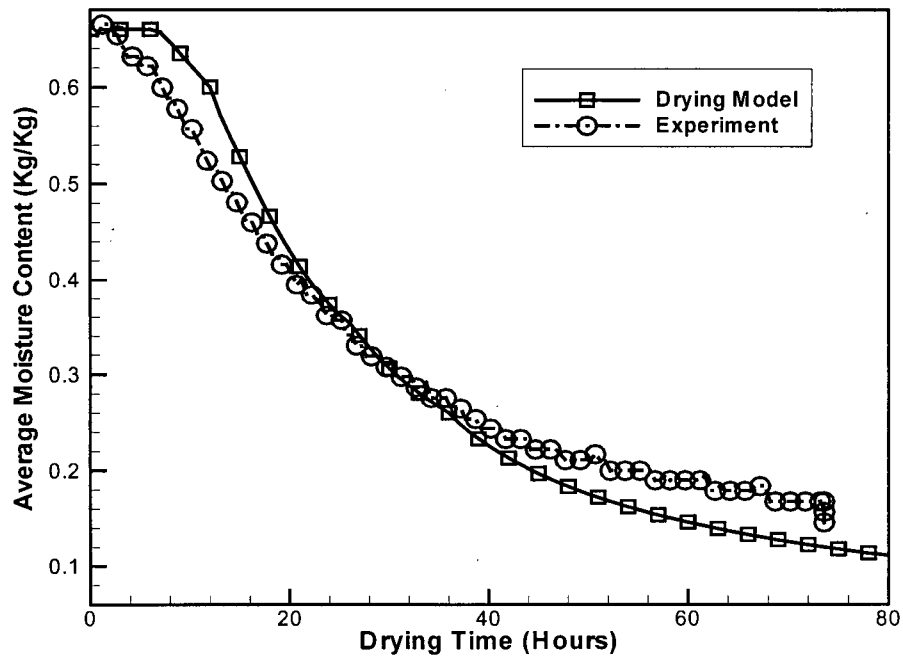


Figure 3.8: Average moisture content as a function of drying time (case 4)

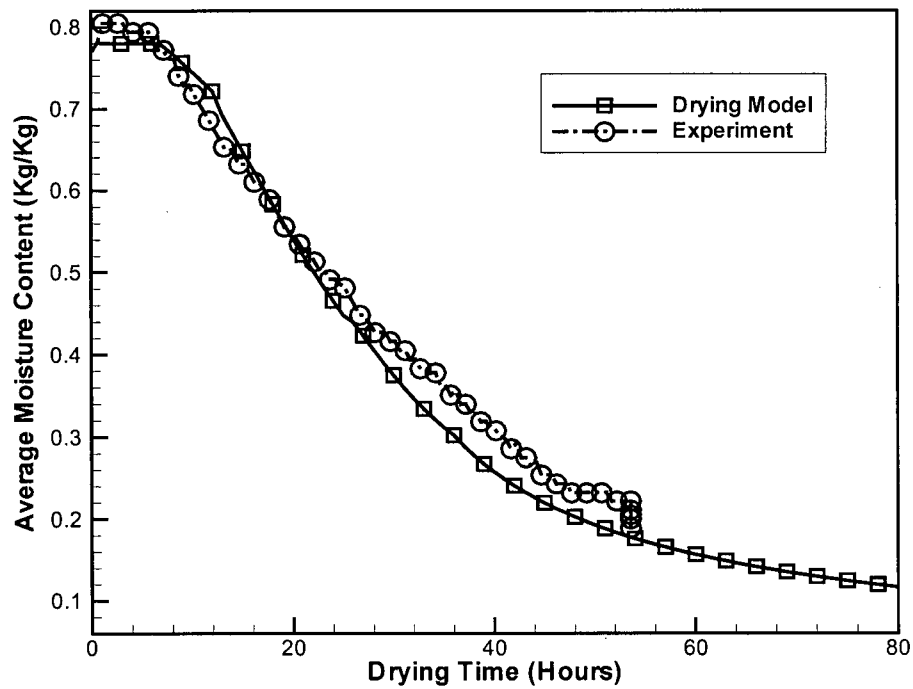


Figure 3.9: Average moisture content as a function of drying time (case 5)

The contour plot of moisture content distribution at different locations inside the lumber is shown in Figures 3.10 and 3.11. It can be seen that the moisture content at the contact surface with the air drops very fast (the thin layer at the surface will be in equilibrium with the airflow very quickly, and the drying is at stage II, see Figure 1.2). After one hour of the drying process, the moisture content at the surface shows a slight increase. This is due to condensation of the water vapor on the surface when the board temperature is still low. During the first few hours, the moisture content at the central line shows a slight drop, but at a rate less than that of the surface. This shows that the liquid water inside the lumber is moving towards the surface at a lower rate than that of the drying rate. The drying front steadily recedes into the center.

Figures 3.12 and 3.13 show the contour plots of the pressure inside the lumber as a function of drying time. From these figures, we can see that during the first few hours of the drying process, the pressure inside the lumber increases. A slightly low pressure is observed near the surface of the wood where the liquid water is extracted by the capillary force (thus causes the expansion of the gaseous volume). As drying progresses, the low pressure has moved inwards towards the center. Both high pressure due to the temperature increase (near the surface) and low pressure due to capillary force can be observed. After a certain time the pressure reaches a maximum at the center, then it decreases. The increase of the pressure is due to evaporation of the free water and the decrease is due to the loss of the free water because of drying. In the model the water vapor is assumed to be in equilibrium with free water if the moisture content is above the fibre saturation point (FSP), and in equilibrium with the bound water if the free water is absent. The result shows that the total pressure inside the lumber could be significantly

larger than the atmospheric pressure, especially for high temperature drying (near or above boiling point). Retaining the pressure equation in the model is not only appropriate, but also necessary.

Contour plots of the temperature inside the lumber as a function of drying time are shown in Figure 3.14 and 3.15. During the constant drying rate period when the free water at the boundary is still present, the temperature of the lumber equals the wet bulb temperature. Once the free water is gone, the temperature shows a second increase, starting from the surface and propagating to the center.

3.4.2 Effect of transport parameters

Effective diffusivity of vapor (D_{eff}): The ability of the gaseous diffusion through the porous media is characterized by D_{eff} . In the domain of liquid migration, the vapor pressure is equal to the saturated vapor pressure for which the gradient is negligible. Thus the effective diffusivity has no influence on drying. But in the domain when no free water is present, the value of D_{eff} directly controls the migration of moisture.

Intrinsic permeability and relative permeability: These parameters describe how easily one liquid can move in a porous media. The values are related to wood species. Softwood has large permeability, therefore it is relatively easy to dry. On the other hand, hard wood has small permeability and will take longer time to dry.

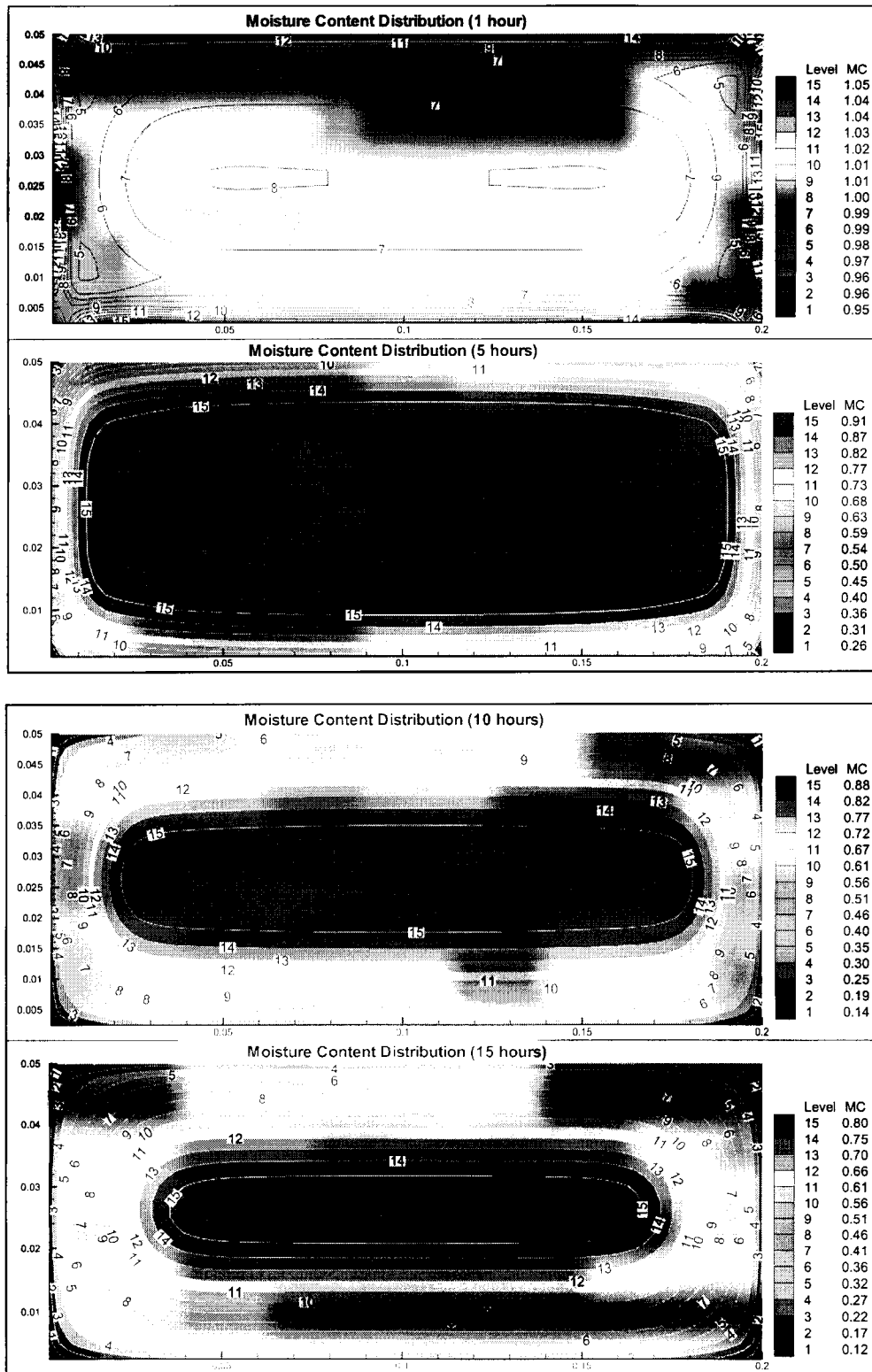


Figure 3.10: Moisture Content Distribution at Different Drying Times (case 1)

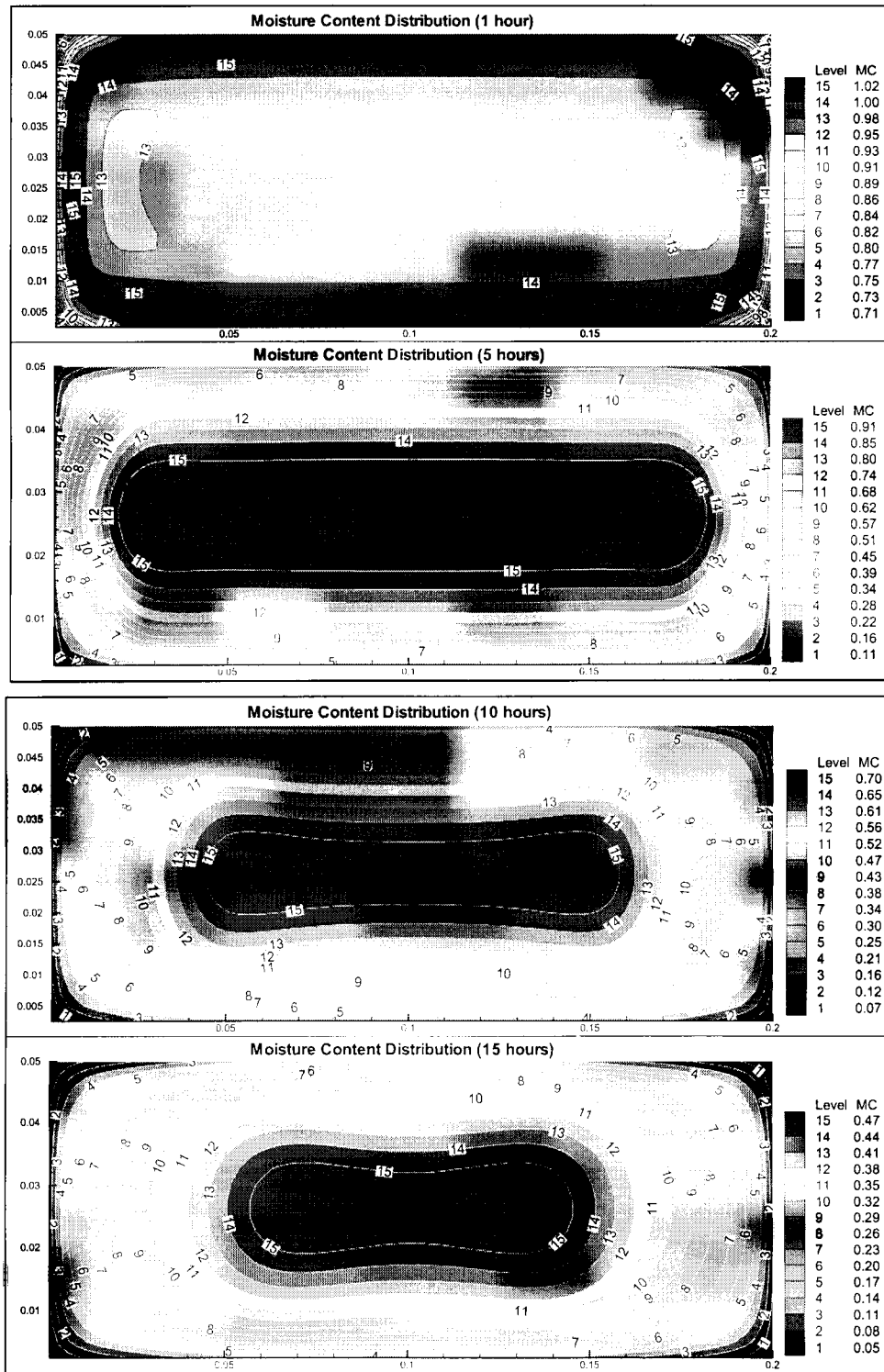


Figure 3.11: Moisture Content Distribution at Different Drying Times (case 3)

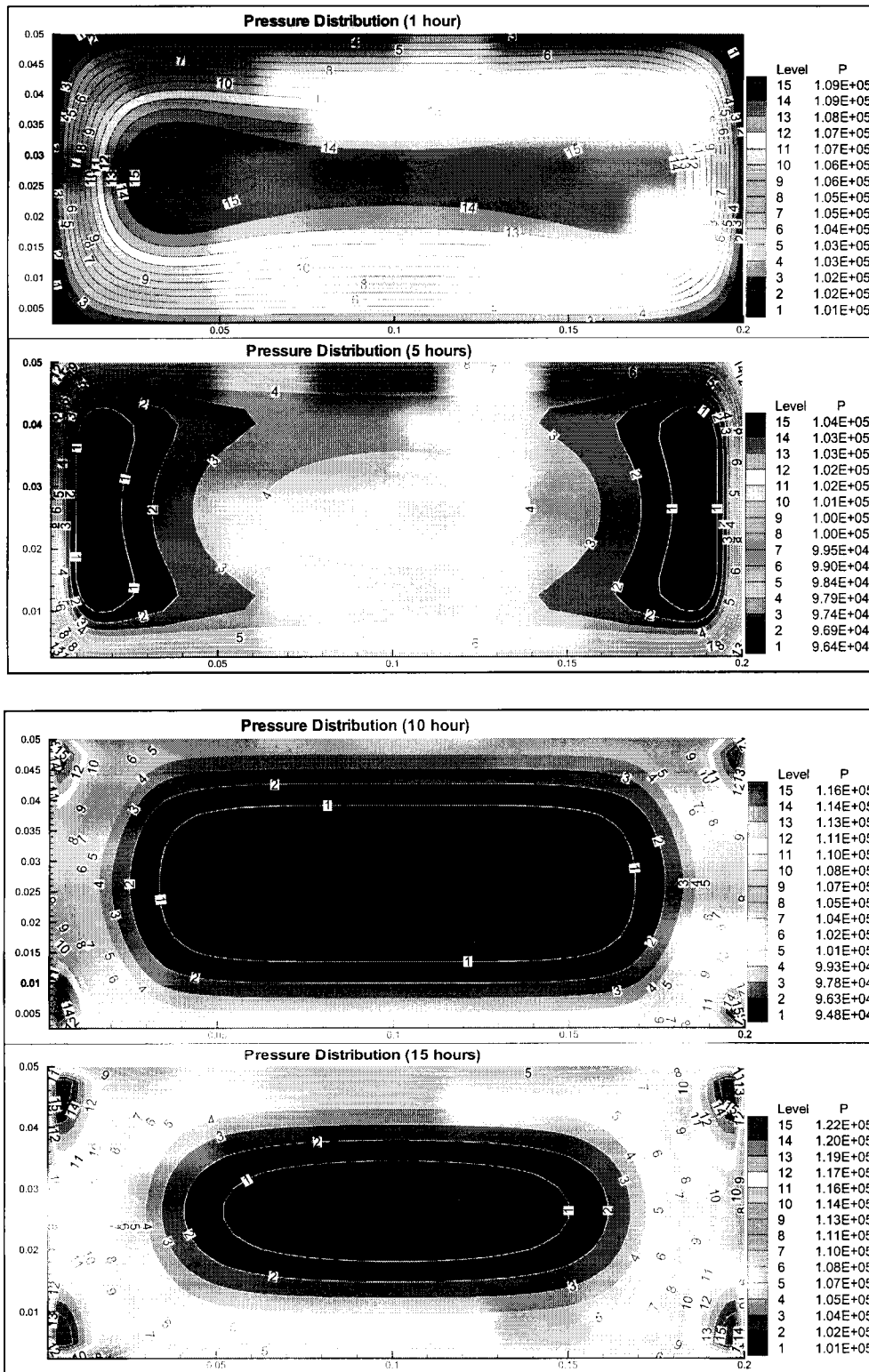


Figure 3.12: Pressure Distribution at Different Drying Times (case 1)

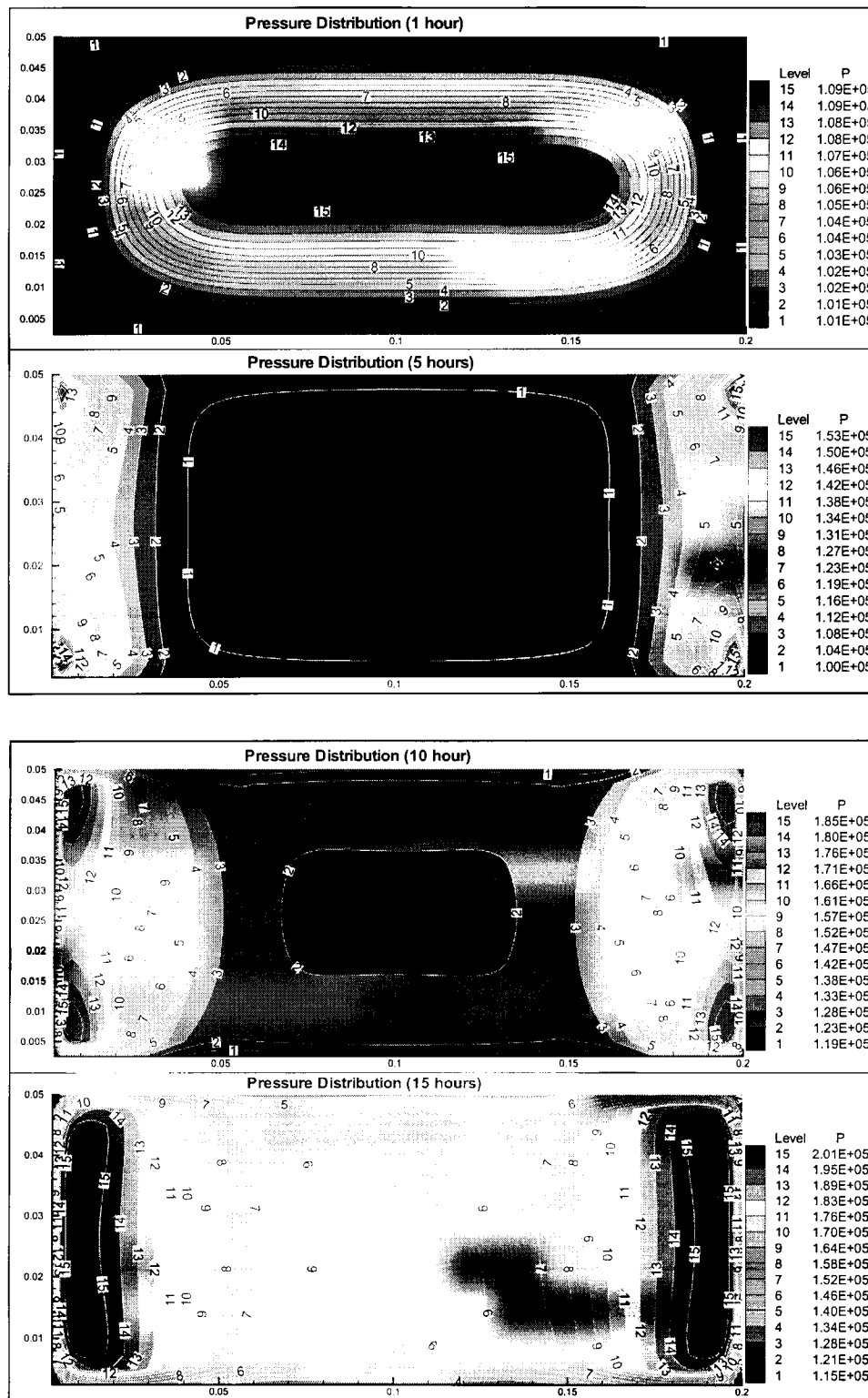


Figure 3.13: Pressure Distribution at Different Drying Times (case 3)

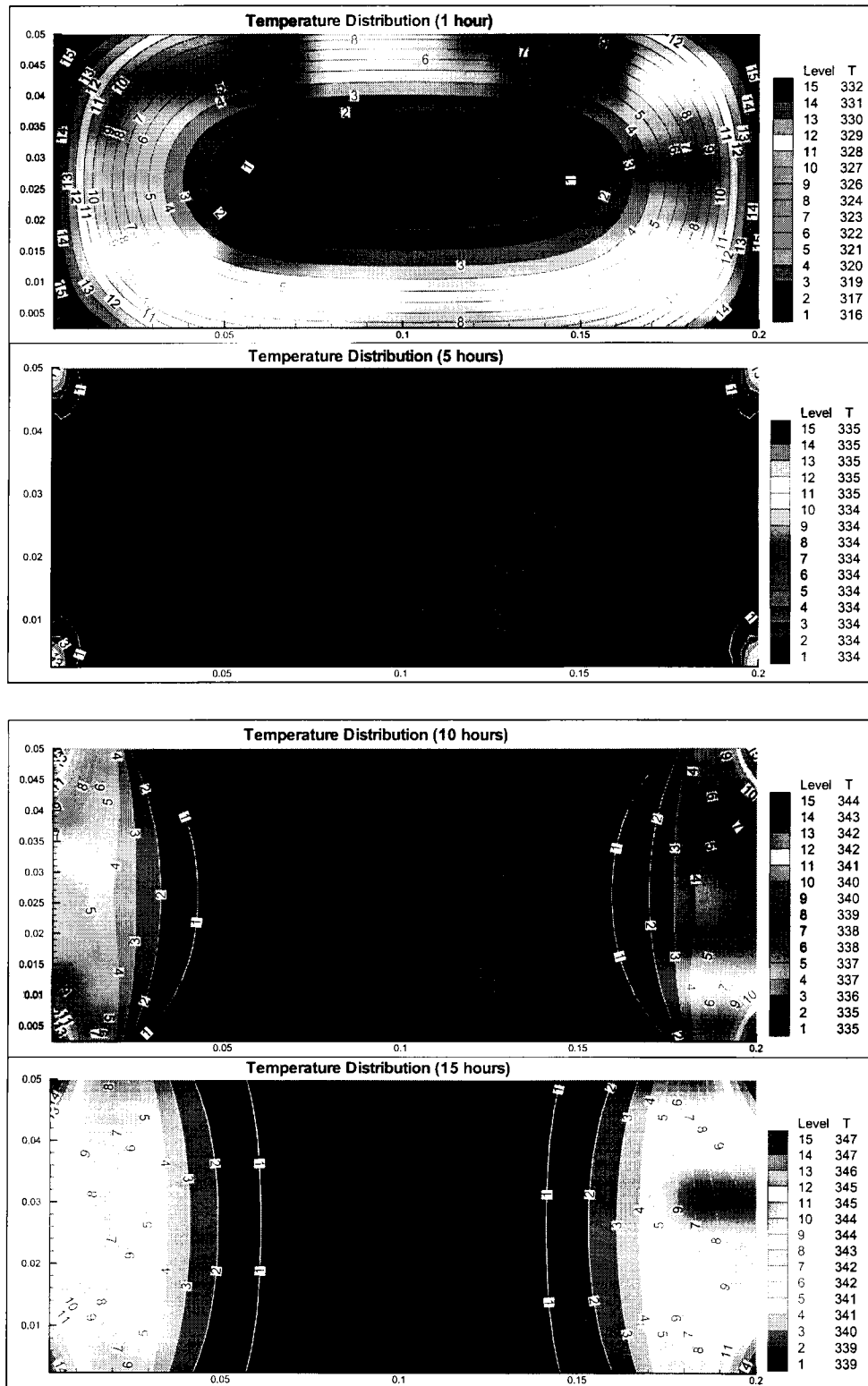


Figure 3.14: Temperature Distribution at Different Drying Times (case 1)

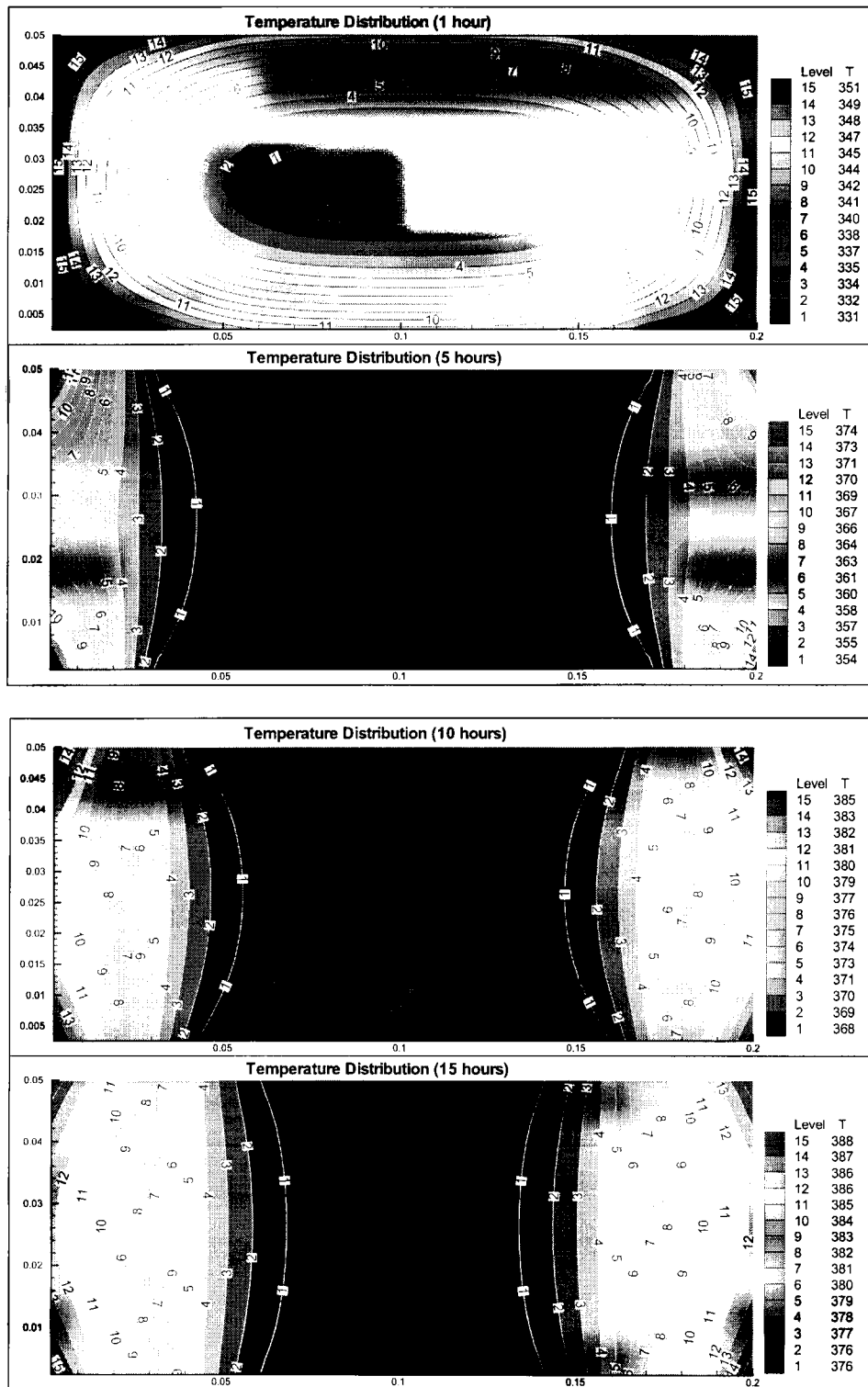


Figure 3.15: Temperature Distribution at Different Drying Times (case 3)

Chapter 4 Coupling of Airflow and Wood Drying Models

4.1 Why the coupling process is needed

A large effort was devoted to the study of the airflow and wood drying models during the end of the last century, and the results have contributed to the industry. However, few people focus on the complete heat and mass transfer process inside a kiln, partly because of the lack of computation power. The results of the separate models can only provide the kiln operators with qualitative information. Other more important information, such as drying time, energy needed and kiln drying schedule, cannot be provided before a kiln drying. With the development of large parallel computer systems, prediction of the complete drying history for lumber population in a kiln is possible.

4.2 Coupling process description

In the present study, the code **CMGFD**, developed by Paul Nowak, was used to carry out the flow field calculation, and the code **WOOD** developed by the author of the thesis was used to simulate the heat and mass transfer inside the wood pieces, and a **CONTROLLER** was used to couple these two parts. Thus we have three working codes: **CMGFD**, **WOOD** and **CONTROLLER**. The code **CMGFD** runs on a PIII node, and **WOOD** runs on 116 nodes, which are for the simulation of 116 wood pieces. The **CONTROLLER**, coded using FORTRAN, can run on any of these nodes or a separate node. Coupling is through the message passing, and the exchange of data on network-mounted disks, such as heat and mass transfer coefficients, temperature, etc. This can be shown in the following Figure 4.1.

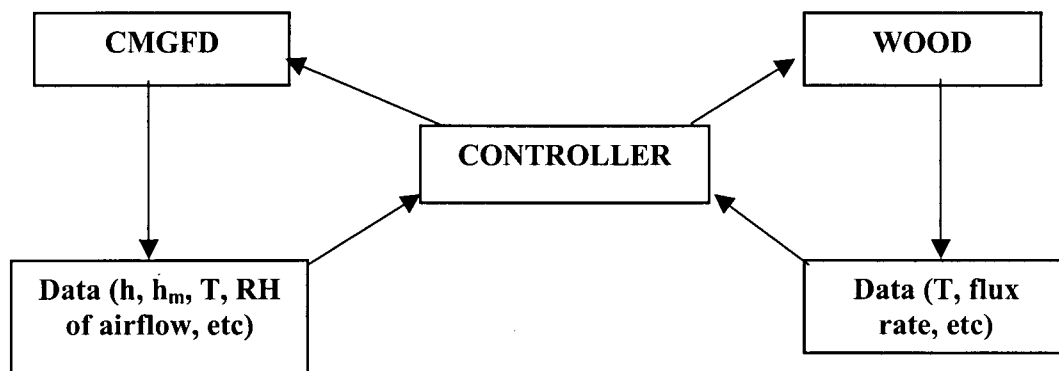


Figure 4.1: Illustration of the coupling process

CMGFD starts first, does a full flow field calculation and outputs the result to a disk file. The CONTROLLER then reads this file and sends the necessary data to WOOD, which starts to run on a fixed number of computer nodes (116, in this case). It periodically sends data to CONTROLLER, which provides CMGFD with the data for carrying out the scalar update for the flow field. These scalars are then transferred back to WOOD through CONTROLLER. The above process repeats many times until a reasonable result is given.

It can be seen that the coupling is a two-way process. The following procedure has been used during development of the code:

- 1) Calculate the flow field variables, such as velocity, pressure, temperature and other scalars. It is assumed to be steady state and will serve as the start-up condition for transient calculations. This flow field remains unchanged for a time interval T_1 .

Velocities and tangential stresses are calculated from this calculation, including heat and mass transfer coefficients based on Reynolds analogy.

- 2) The output of these calculations has been used by the transient calculations which calculate the following: the heat and mass transfer were calculated in the wood in chosen positions in a transient way. All lumber pieces were included in the present study. The boundary conditions were established by using data resulting from the flow calculations: the convective boundary conditions were used at the boundary for the heat transfer calculation.
- 3) For the heat and mass transfer calculations outside the wood (i.e., in the airflow) we solve the temperature and vapor content as a transient species equation using scalars. The transport equation with the convective and diffusive terms was calculated. To minimize computation time involved in the solution of the momentum equations (coupled PDEs), the velocities used are the ones computed in the quasi-steady state. The vapor concentration and temperature of the air are necessary to solve the mass and heat transport equations in the wood. These transient calculations have to be carried out for the complete cycle of drying.
- 4) In the future the flow equations might be solved again to take into account the resulting densities from the moisture calculations, and the temperature field can be calculated again based on that.
- 5) The velocity field is reversed to simulate the fan reversal inside a commercial kiln. Because of the long computation time required to get a flow field convergence, we simply changed the flow field without considering the convergence process involved.

- 6) Message Passing Interface has been used to provide a parallel computation platform for the code. A detailed description can be found in Chapter 4.3.

Time step:

Three important time intervals have been used in the calculations.

T1: the time interval for recalculating the flow field (including mass, momentum and scalar equations for airflow). Since the flow field might change during the drying process (which we don't know exactly), we need to redo the airflow calculations at a suitable time. This time interval is relatively large since airflow calculation is very time-consuming. Typically a complete flow field calculation will take more than 8 hours, depending on the kiln size and grid. So there are from 2 to a maximum 5 recalculations. This re-calculation has not been done in the present study. With the increase of the computation power in the UBC Physics Department, we may be able to do this in the near future.

T2: the time interval for exchanging data between WOOD and CMGFD. Typically the time interval for recalculating the scalar equations of CMGFD will not be the same as the time step of WOOD. The former is longer than the latter. Proper ways of choosing the time interval are to be determined. The value used at present is about half an hour during the early drying stage, and 1 hour during the later stages.

T3: the time step for WOOD. This value is relatively easy to determine. It is from several seconds in the first few hours during the convective drying stage, to several minutes during the diffusion drying stage.

Heat and mass transfer:

At any time during the drying process, water vapor dumped by the wood will go into the airflow and be carried out. Airflow provides the wood pieces with energy for drying. There has to be a mass balance and a heat balance inside the kiln. This is controlled through data exchanging between CMGFD and WOOD. Suppose during time step t_i to t_{i+1} , the wood moisture content changes from MH to ML, then the air has to get water vapor of the amount $(MH-ML) \times (\text{Mass of Oven-Drying-Wood along the exchange surface})$. This is difficult to implement, however, since we do not know the value while another calculation is being carried out. To solve this, we have used the flux rate at a previous time step. Opening of a vent is considered. Heating coils will be modeled as a heat source. The condensing of the water vapor is not considered at this time. Energy loss due to leakage might be considered in the future.

Partition of mass and heat exchanged:

Unless we match the time step as well, we will have to do a partition on the heat and mass exchanged. Suppose the time interval for the airflow scalar calculation is 5 minutes, and the time step for the wood drying model is 1 minute. We will have to divide anything from airflow into five parts (which may or may not be equal). The division may be related to drying rate. Every five parts from the wood drying model will be added together to be given to the airflow. At present, equal division is used.

Grid consideration:

There are two codes involved in the calculation, and the CPU time needed for each code cannot be exactly the same. We have to pay attention to the grid matching, since we

should not have one code sitting there idle for too long. Currently the two codes use different grids, and interpolation of the data has been used. This is coordinated through the CONTROLLER. It is a trial and error process and we do not yet have an optimized scheme.

Other Considerations:

1. The gaps between lumber pieces and board irregularities will be modeled as source and sink term in the future computation. This would be based on previous calculations for the gaps
2. This code will definitely need a lengthy CPU time. It is impossible to finish the project with only two computers. I have to use parallel methods. The Message Passing Interface is introduced in Chapter 4.3. Wood pieces at certain locations may be selected for calculation to reduce the total computation time. This leads to an additional problem: at which point should lumber pieces be selected, and how should the result be interpolated. For simplicity, we have included all the wood pieces for the present study.

4.3 Message Passing Interface (MPI)

The goal of the Message Passing Interface, simply stated, is to develop a widely used standard for writing message-passing programs. As such the interface attempts to establish a practical, portable, efficient, and flexible standard for message passing.

The computer system can be shown as follows:

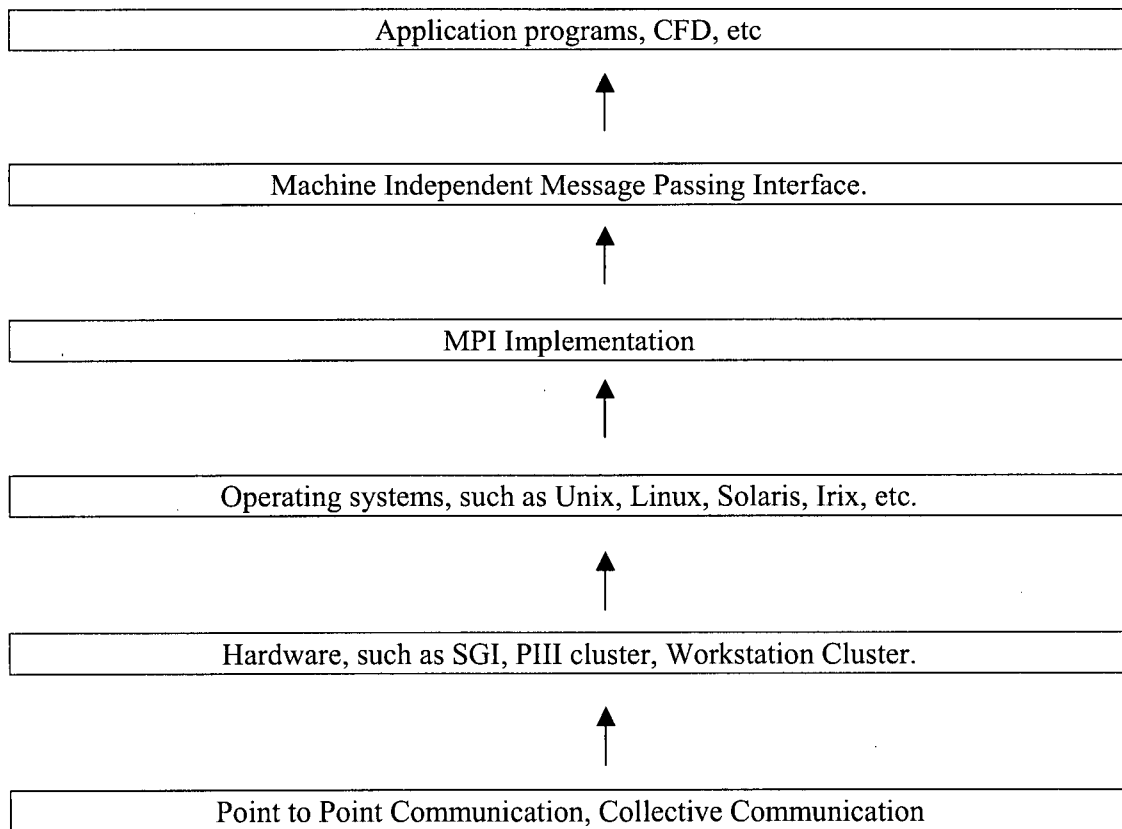


Figure 4.2: MPI and Computer System

There are two basic methods for interprocess communication:

- Shared-memory method.
- Message-passing method.

In message-passing systems, there are two basic primitives for interprocess communication: **send** (address, data) and **receive** (data). The sending process generates the data to be shared and sends it to the recipient(s) with which it wants to communicate. The recipients(s) receive the data.

The **send** and **receive** primitives can be divided into two types: block and non-block. In block communication, the process which initiates the call has to wait for an acknowledgement from its destination process. This is a waste of CPU time and should be avoided.

The shared-memory method provides to processes in a system with a shared address space. Processes use this address space in the same way they use normal local memory.

The use of a shared-memory method for interprocess communication is natural for distributed process running on tightly coupled shared-memory multiprocessors. However, for loosely coupled distributed systems, no physically shared memory is available to support the shared-memory method for interprocess communication. Thus, MPI is mainly used in loosely coupled systems.

4.3.1 Collective Communications

A communication pattern that involves all the processors in a communicator is a collective communication. The sending and receiving of the messages between nodes can significantly influence the efficiency of the algorithm. Suppose we have eight nodes, and

we need to send information to all these computers. The data is on node 0. We can send the data from node 0 to node 1~7. This collective communication is called a broadcast. It will become inefficient as the number of nodes and data size increase. An improved method is tree-structure communication as illustrated in the following figure:

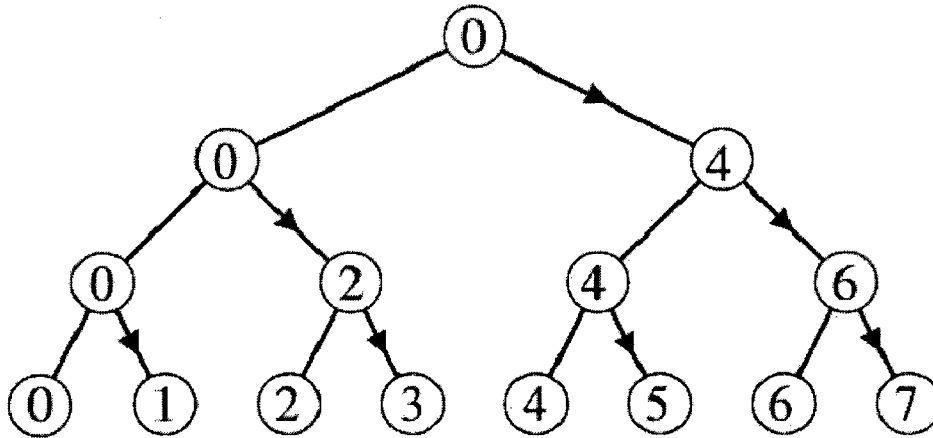


Figure 4.3: Collective Communication

We can chose:

1. 0 sends to 4.
2. 0 sends to 2, 4 sends to 6.
3. 0 sends to 1, 2 sends to 3, 4 sends to 5, 6 sends to 7.

We might also have chosen (for example):

1. 0 sends to 1.
2. 0 sends to 2, 1 sends to 3.
3. 0 sends to 4, 1 sends to 5, 2 sends to 6, 3 sends to 7.

There are other collective communication methods [27] which are beyond the scope of the research work.

4.4 Results and discussions

In the present study, the calculation was carried out for a typical kiln. The grid layout and the velocity distribution of the same kiln can be found in Chapter 2. There are four wood packages, which will be referred as package 1, 2, 3 and 4 (see Figure 4.4). Packages 1 and 2 are also referred to as top package and bottom package, respectively. They will be referred to as left side packages (1 and 2) and right side packages (3 and 4). Lumber pieces were numbered from 1 to 116. The initial moisture content for all lumber pieces is 100%. At present, one 2D case is investigated.

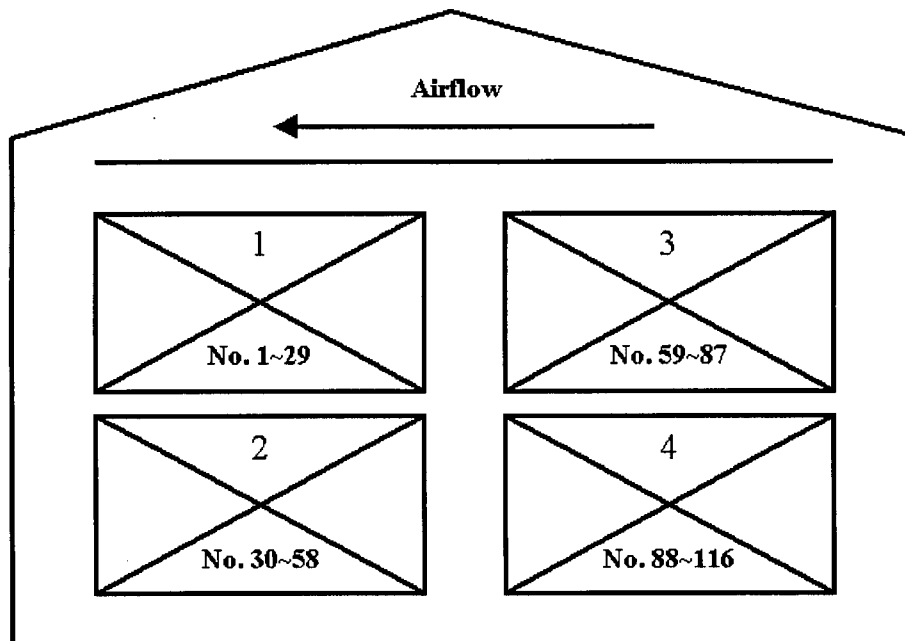


Figure 4.4: Simulated Wood Kiln

Figure 4.5 shows the contour plot of the temperature inside the investigated woodkiln at different times. Figures 4.6 and 4.7 show the temperature along the centerline of each channel. It can be seen from the figures that the unevenness of the airflow has resulted in

a temperature gradient inside the kiln. The left side of the kiln (packages 1 and 2), through which the air goes into the stacks, has a higher temperature. On the other hand, the right side has a lower temperature. Even on the same side, the temperature is different at different flow channels. Package 2 (bottom stack) has a higher average temperature than package 1 (top stack). As explained in Chapter 2, the slanted roof causes the flow to accelerate before entering the plenum, thus providing the bottom stack with more airflow, which results in a higher temperature at the bottom. Airflow in the gaps between packages has a higher temperature because of reduced airflow resistance.

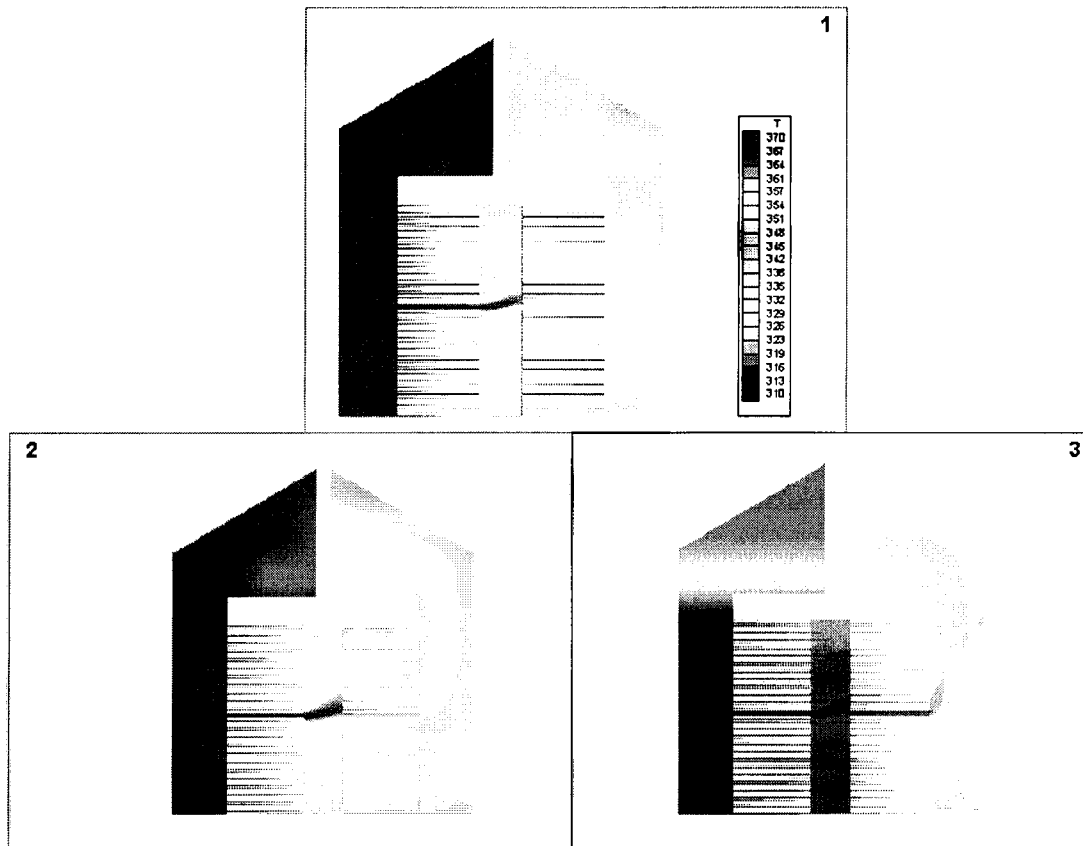


Figure 4.5: Temperature inside a typical woodkiln at different times

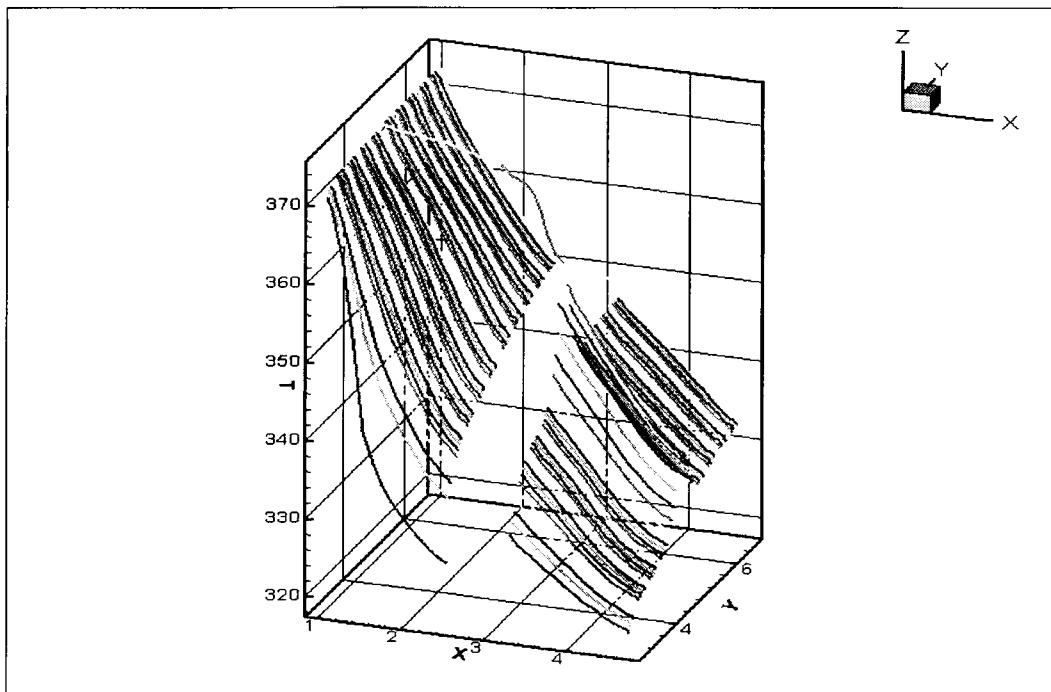


Figure 4.6: Temperature along the centerline of each channel (3D-Surface)

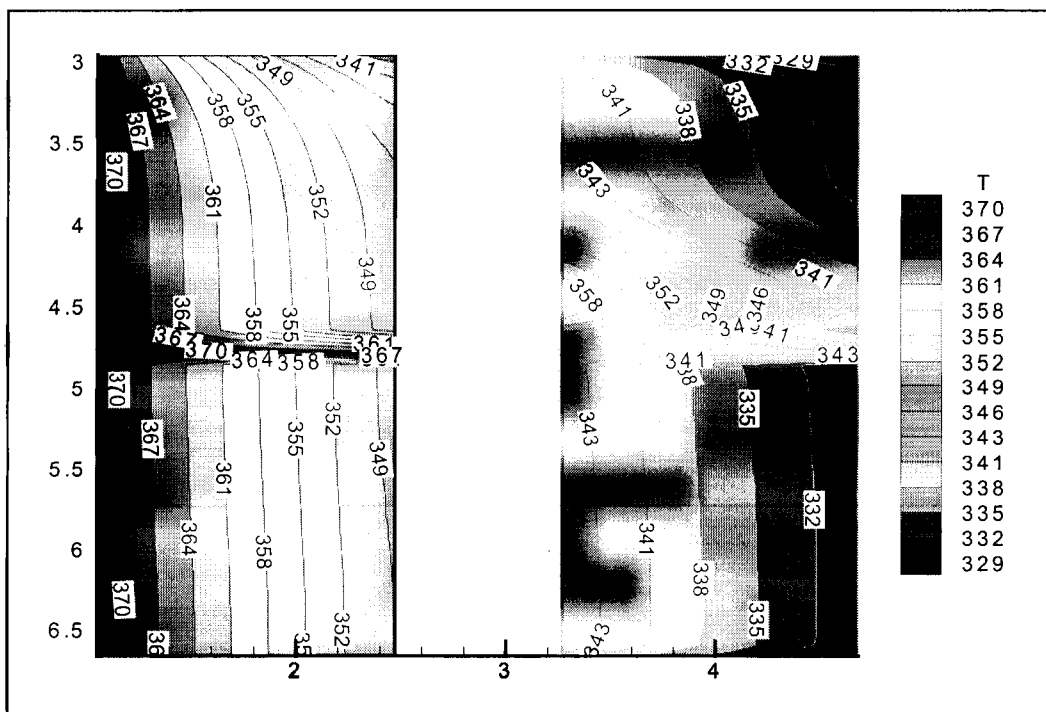


Figure 4.7: Temperature along the centerline of each channel (2D-Contour)

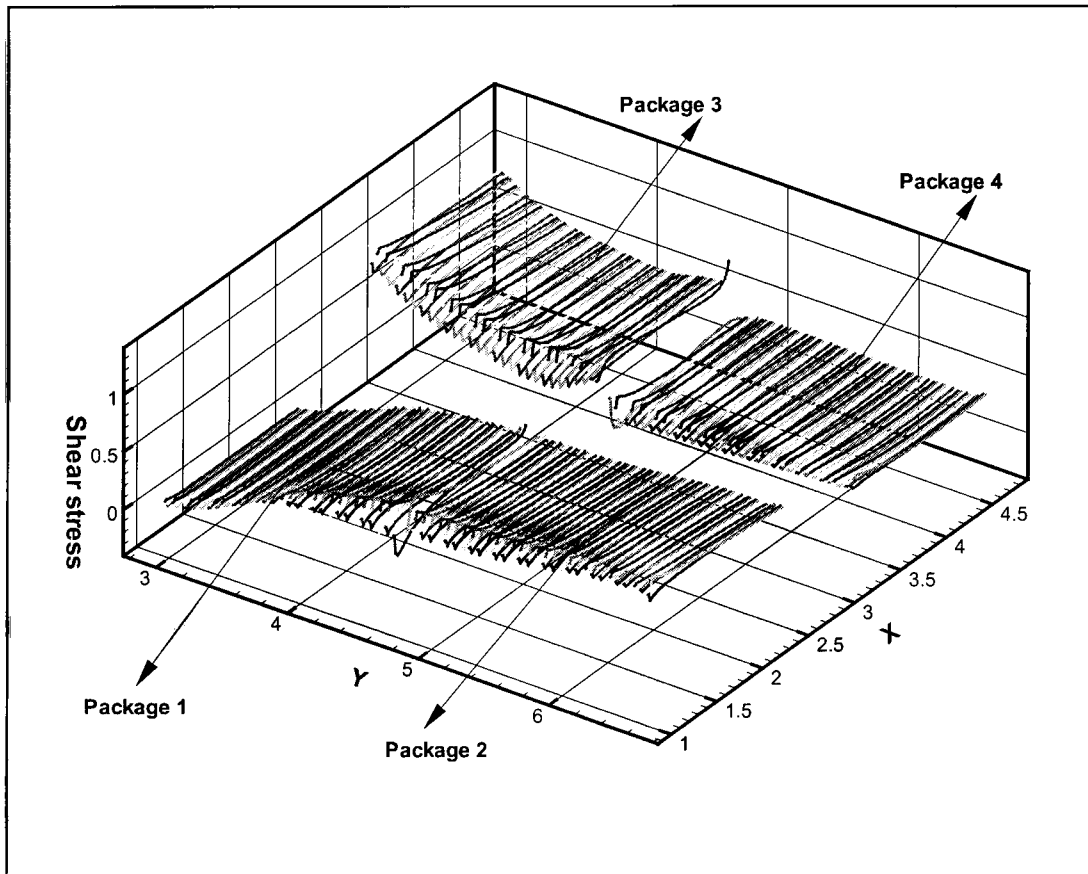


Figure 4.8: Shear stress at the boundary (Pa)

Figures 4.8, 4.9 and 4.10 show the shear stress at the boundary. The increasing X direction is from left side to the right side of the kiln (stream-wise). The increasing Y direction is from the top stack to the bottom stack. It can be seen that the bottom stack has a larger shear stress than the top. The reason for this is that the bottom stack gets more airflow due to the slanted roof which causes the flow to accelerate before entering the package, and the flow pattern is altered in the lower region. In each channel, the shear stress is normally larger at both ends than in the middle. The shear stress is larger at the top surface (TAU2) than at the bottom surface (TAU) for package 2, but smaller for package 3.

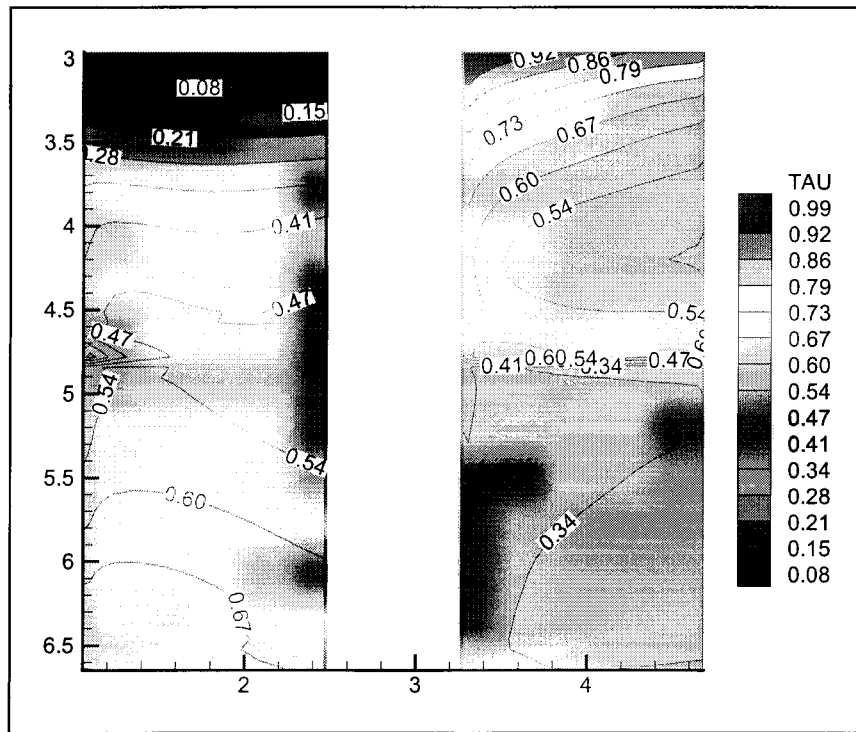


Figure 4.9: Shear Stress at Channel Top (Pa)

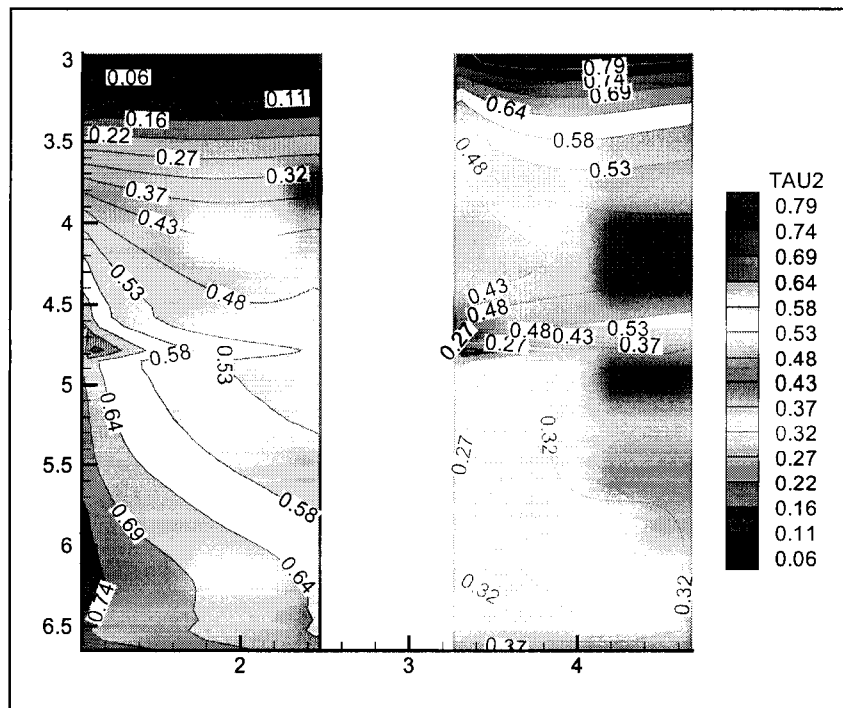


Figure 4.10: Shear Stress at Channel Bottom (Pa)

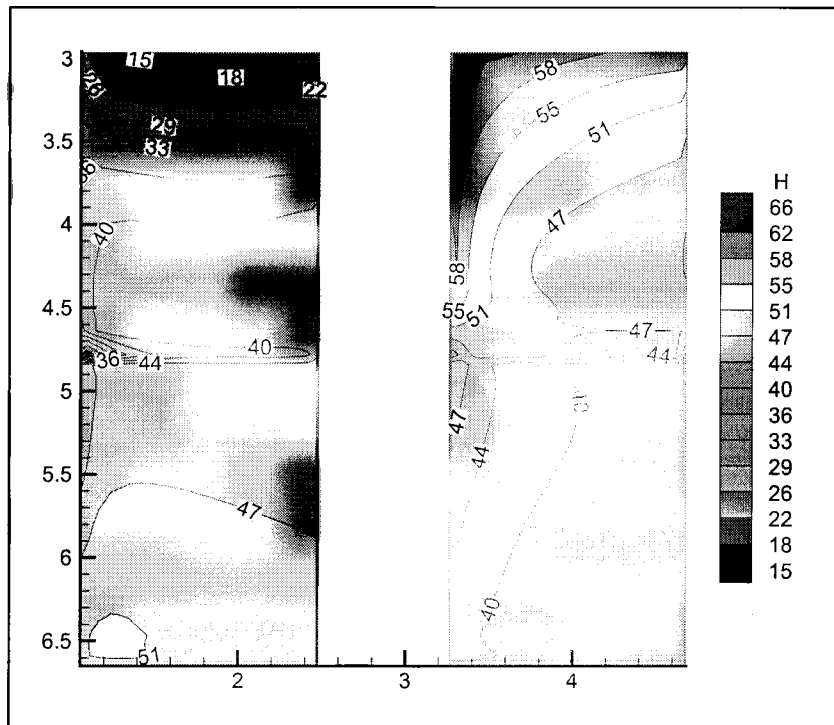


Figure 4.11: Heat Transfer Coefficient at Channel Top

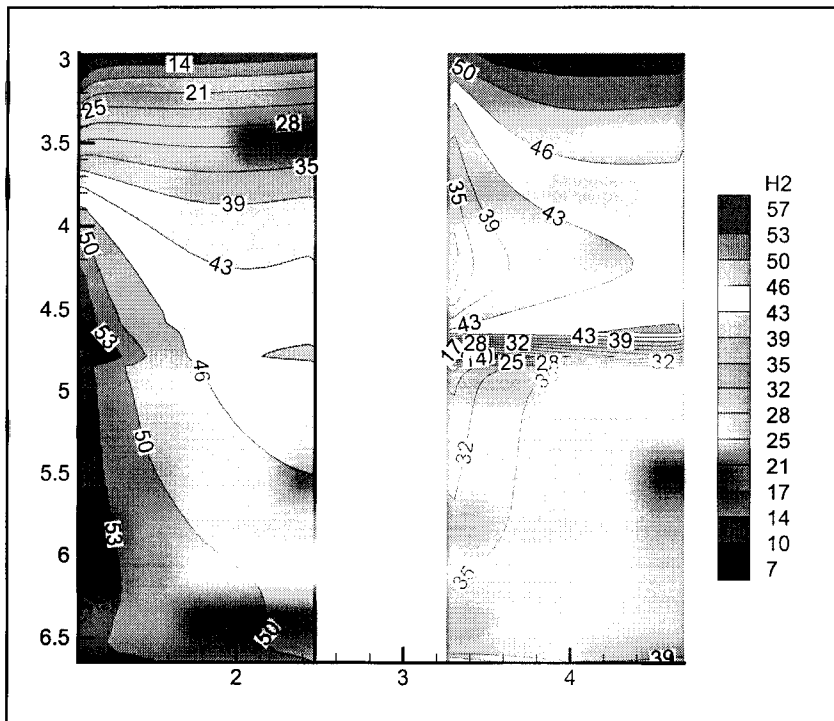


Figure 4.12: Heat Transfer Coefficient at Channel Bottom

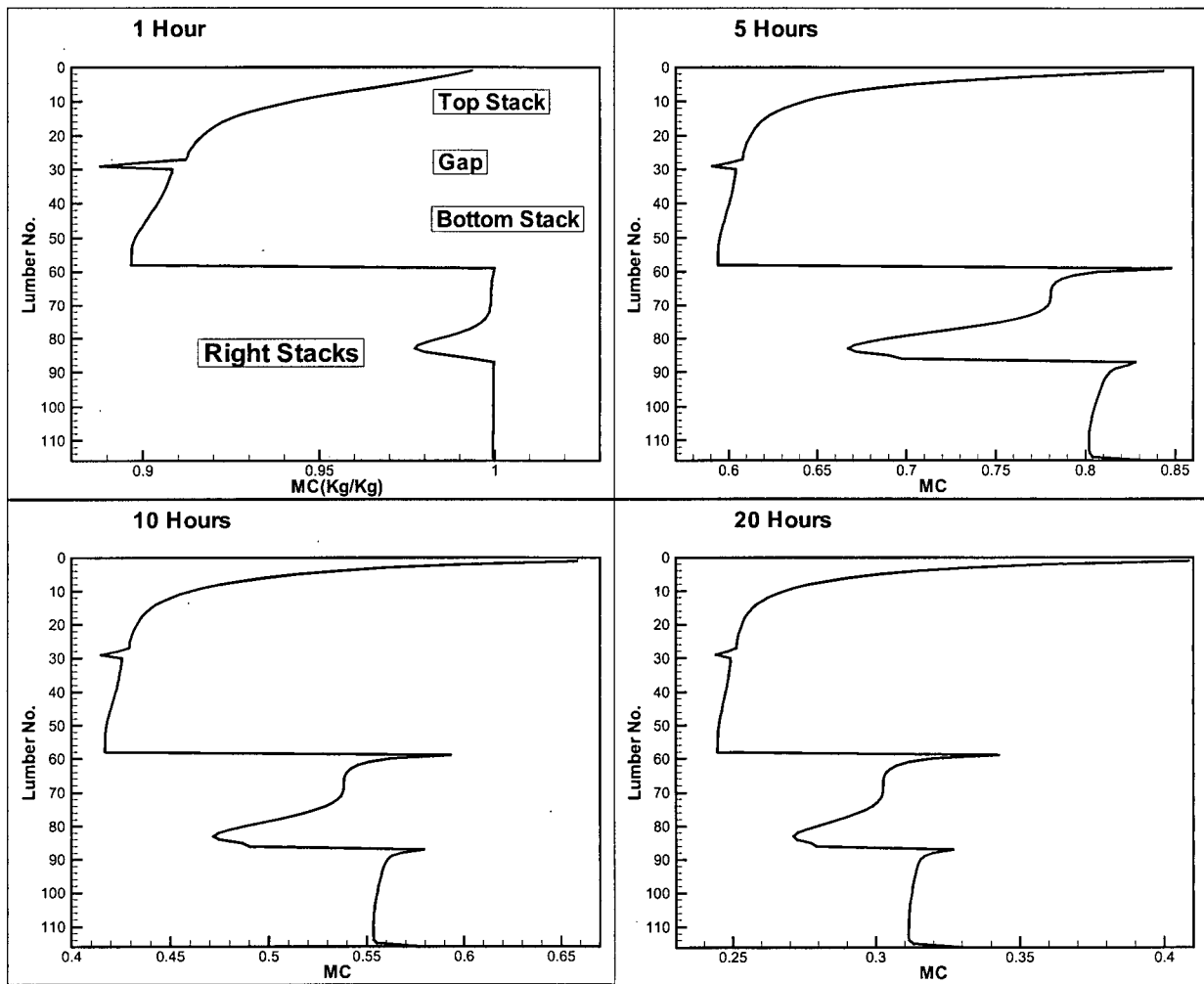


Figure 4.13: Average moisture content distribution

Figure 4.13 shows the average moisture content distribution of 116 lumber pieces inside the investigated woodkiln. No. 1 to 58 is from the two stacks on the left side (packages 1 and 2), and the rest is from the right side. All these lumber pieces start at the same initial moisture content. It can be seen that the lumber pieces dry faster at package 2 (left bottom) than at package 1 (left top). Lumber pieces in package 3 (right top) dry faster than package 4 (right bottom). The lumber pieces also dried faster near the gaps, which enable them get more airflow because of the reduced flow resistance.

The average temperature distribution of the lumber pieces is shown in Figure 4.14. The characteristic is almost the same as that of the moisture content. The temperature of the bottom stacks is higher than that of the top. Lumber pieces near the gaps have a higher temperature than other pieces.

The phenomenon can be explained by temperature and heat/mass transfer coefficients distribution in Figures 4.7, 4.11 and 4.12. These are related as noted in equations 2.1, 2.2 and 2.3.

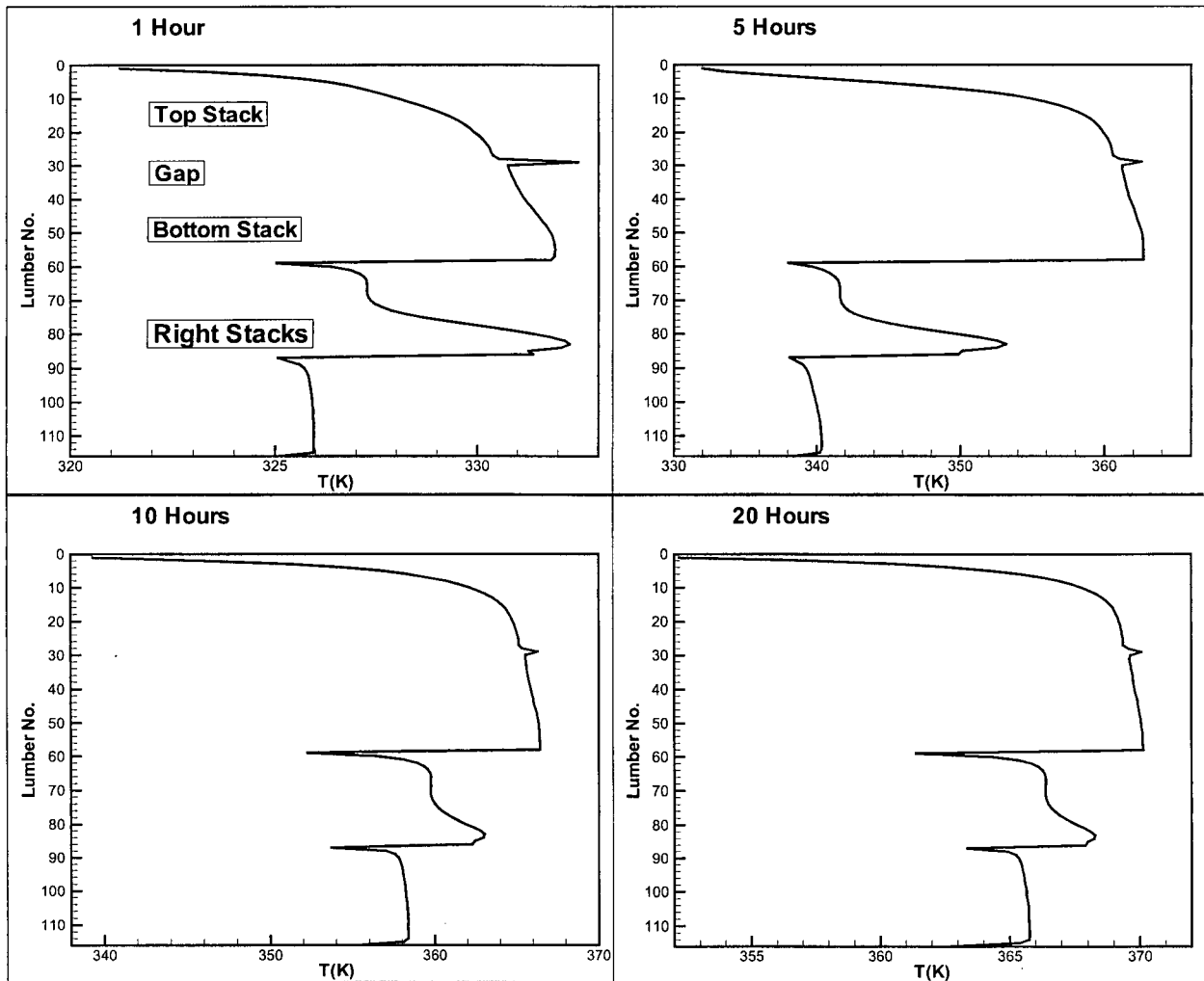


Figure 4.14: Average temperature distribution

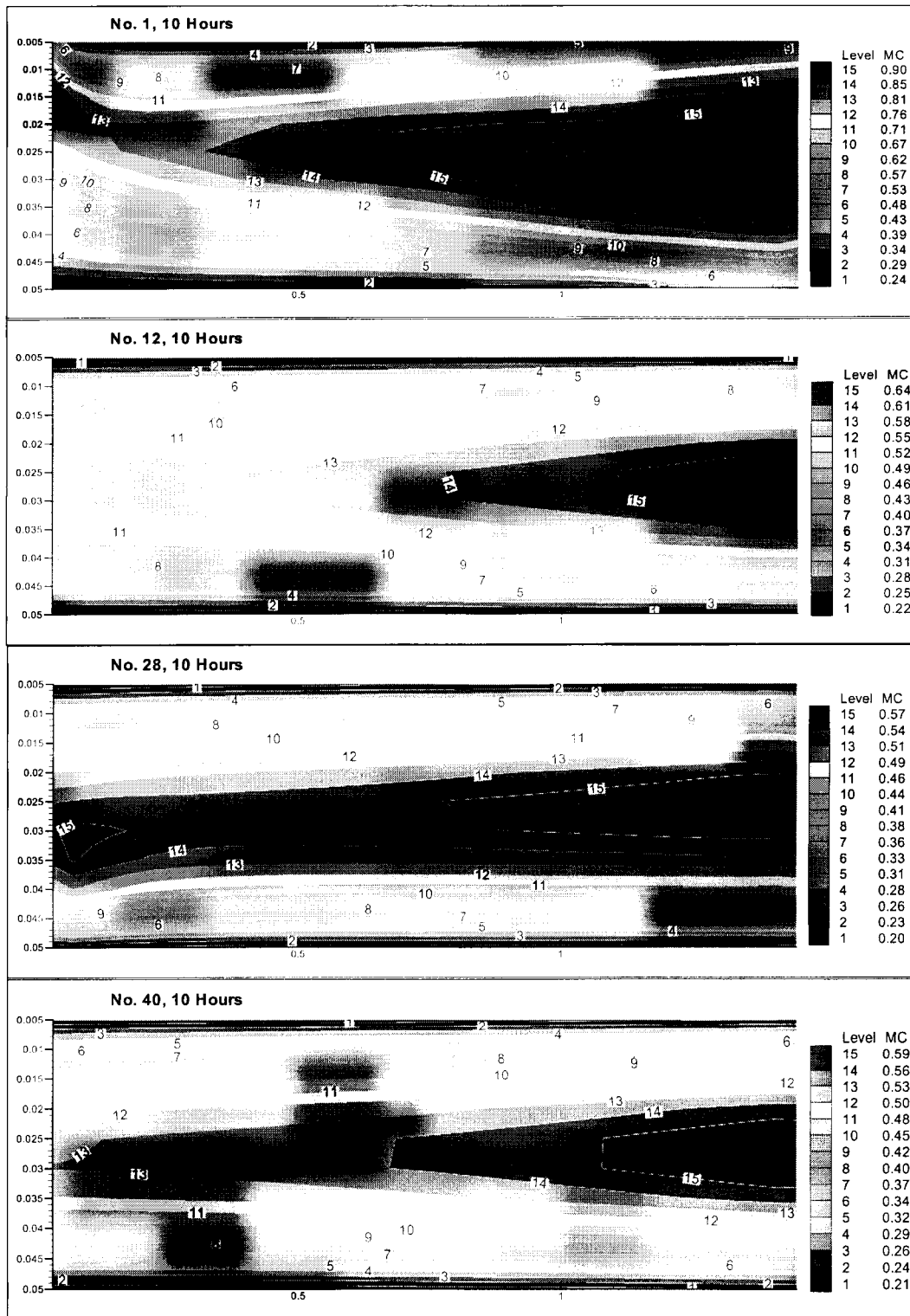


Figure 4.15: Moisture Content Distribution for No. 1, 12, 28 and 40

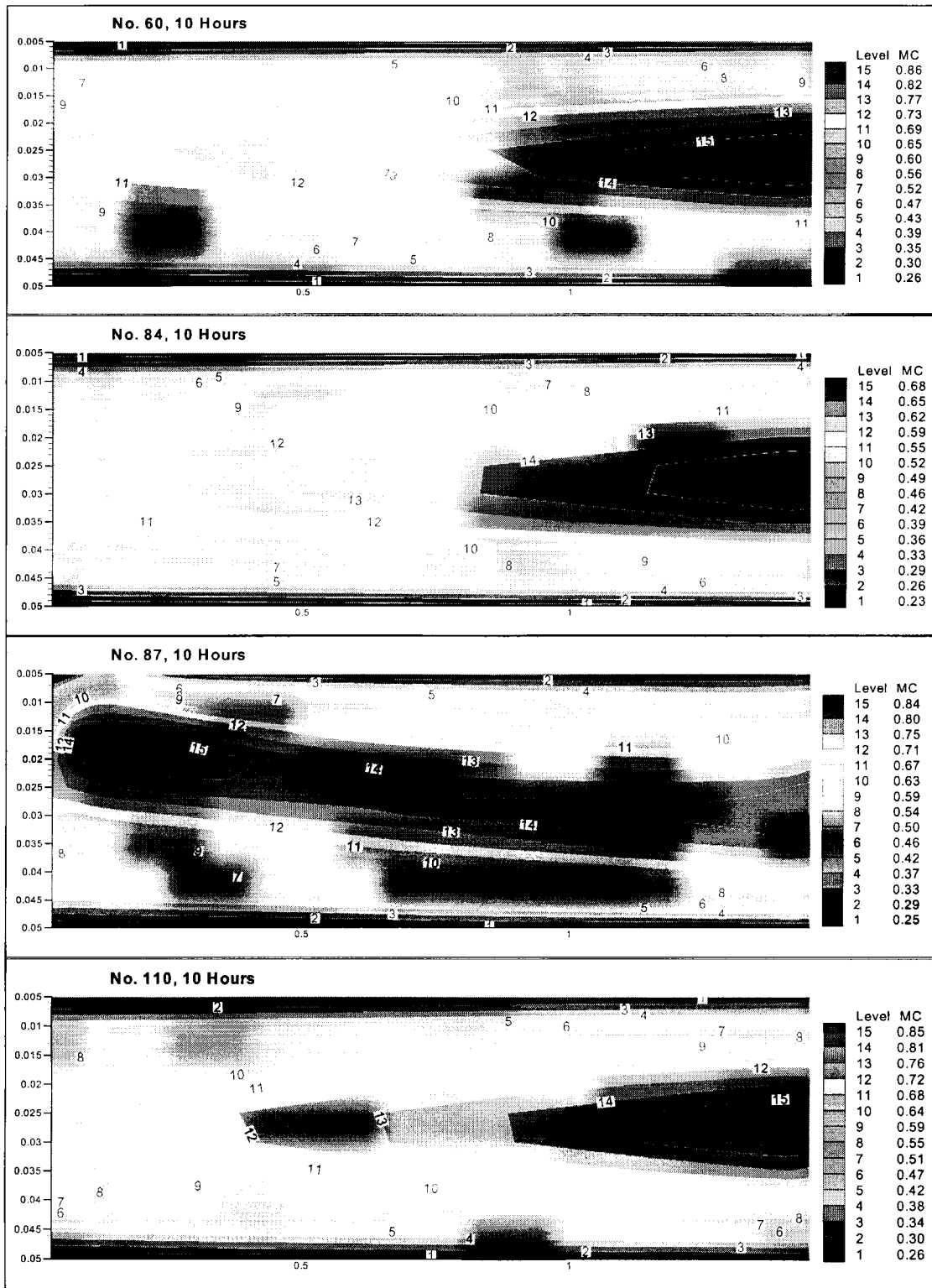


Figure 4.16: Moisture Content Distribution for No. 60, 84, 87 and 110

Figures 4.15 and 4.16 show the moisture content distribution of eight selected lumber pieces (from typical positions inside the kiln) at 10 hours during the drying process. It can be seen that the average moisture content and the moisture profile for lumber pieces at different locations could be significantly different. Even within one lumber piece, the moisture content can have a large non-uniformity. Lumber piece No. 1, which received less airflow due to the low pressure, as described in Chapter 2, dried much slower than any other lumber pieces on the same side. No. 84 dried faster than other lumber pieces on the same (right) side because of the effect of airflow from the gap on the left side (see Figures 2.5a and 4.7). All lumber pieces dry faster at the inflow sides because of the relatively higher temperature and lower airflow humidity.

Large temperature gradients as shown in Figures 4.5, 4.6 and 4.14 can be reduced by reversing the fan periodically. Figure 4.17 shows the result of a simulation of the fan reversal (number 1 to 4 represent different time periods during the reversing process). This is done by retaining the temperature field and reversing the flow field at a certain time. It is hoped that by alternately subjecting all packages to a high temperature and low moisture airflow, non-uniformity in final moisture distribution can be reduced. The completed reversing process has not yet been simulated.

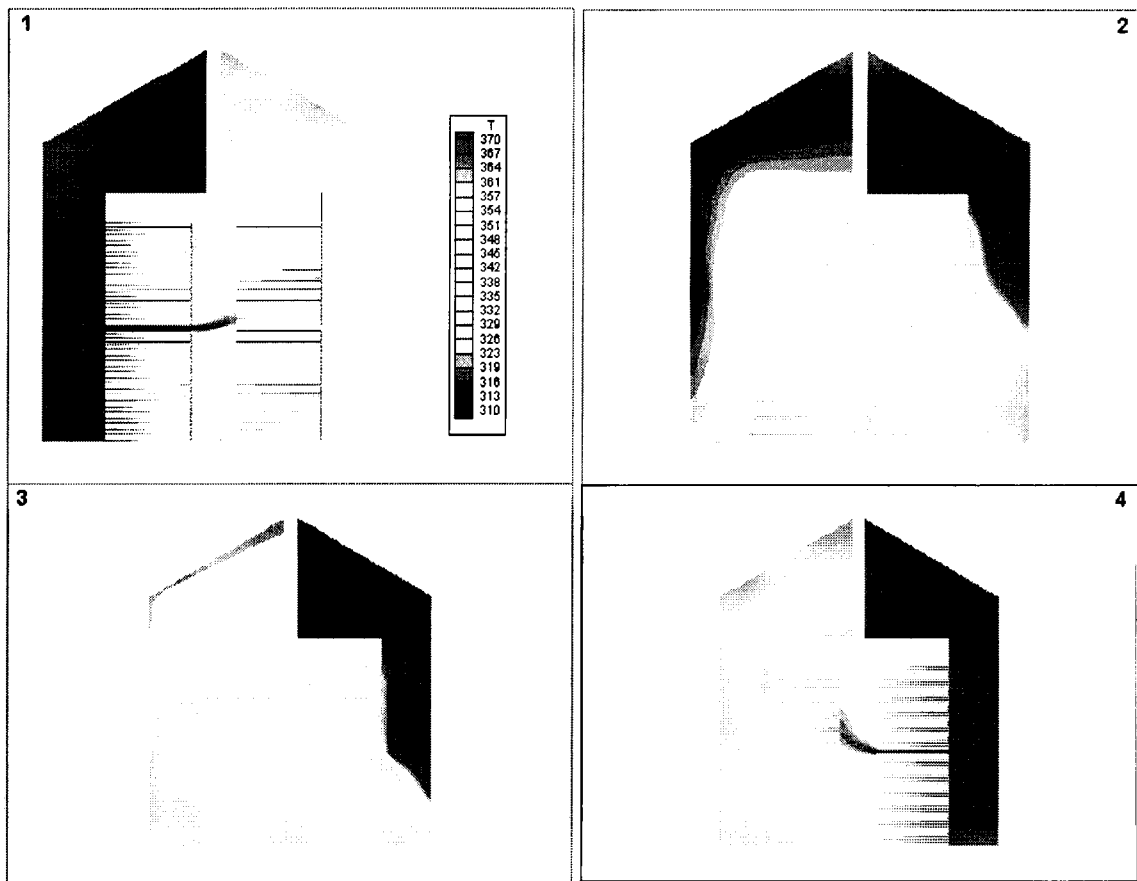


Figure 4.17: Temperature in Flow Field Reversal Case

Chapter 5 Conclusions and Recommendations

5.1 Conclusions

In order to predict the air velocity in each part of a typical kiln, the three-dimensional incompressible Reynolds averaged Navier-Stokes equations [59] governing fluid flow are solved [17]. The airflow model has been modified to investigate the effects of gaps and board irregularities. The model of heat and mass transfer in porous media proposed by Whitaker (and later revised by Perre and Morne) has been revised to take into account the effect of the movement of free water, bound water and water vapor. Above fibre saturation point (FSP), Darcy's law holds for liquid water movement. Below FSP, Fick's law holds for bound water movement. The total pressure in the gaseous phase, which is often assumed to be at atmospheric pressure in the literature work, is observed to be significantly higher than 1atm for some time period. The model provides a good description of the complete drying process and can now be used to improve drying efficiency and product quality. The integrated model of the airflow and wood drying currently in development investigated the drying process of lumber pieces under different airflow conditions in a kiln, the effect on the airflow and the final moisture distribution within a lumber piece and the wood package. It has demonstrated the ability to predict the complete kiln drying process and will constitute a powerful tool to optimize the design and operating of drying kilns.

The integrated model has been applied only to one geometric configuration of kiln and lumber and one species of wood. Without difficulty, the model can now be used to investigate other geometries and other wood species.

From the present single application, the following conclusions can be drawn:

- Irregularities in lumber thickness lead to non-uniform drying. The present model can quantify this effect.
- Gaps between adjacent pieces of lumber can reduce the drying time but also introduce non-uniformity of drying if the gaps are irregular. In addition, gaps reduce the volume of wood which can be dried in the kiln.
- The present model shows that, for the geometry investigated, packages of lumber dry at quite different rates and the individual pieces within the packages also dry at different rates. This quantitative information can be used to redesign the package locations or the plenum sizes in order to change the geometry of the kiln or the location of the packages to produce a more uniformly dried product. The model can be used to explore various alternatives, and to optimize the geometric arrangement of the kiln and the drying schedule (fan reversal, temperature and humidity schedules, etc).
- The present model can also be used to explore the efficiency of new kiln designs or arrangements of wood packages.

5.2 Recommendations for Future Work

The current work has established a method to investigate the wood drying process in a kiln. However, due to limited time, there are still unsolved problems, among which are:

- 1) The effects of gaps and board irregularities have been investigated but have not yet been integrated completely with the wood drying model. It is impossible to include all the gaps because of the large number of gaps involved. Some simplification has to be made before the calculation.
- 2) During the first few hours of kiln drying, the water vapor may condense at the surface of the lumber pieces due to the uneven distribution of the airflow humidity and lumber temperature. This condensation is not included in the model and should be taken into account in the future.
- 3) To simplify the simulation, it is assumed that the airflow pattern does not change during the drying process except the fan reversal. But the three kinds of water movement throughout lumber drying affects the relationship between air velocity and drying efficiency. During the first stage of the drying process rapid surface evaporation dominates and the air velocity needs to be high; during diffusion drying stage air velocity does not need to be as high. Thus, at any stage of drying there is an optimum air velocity. Too low a velocity will waste kiln capacity and increase heat loss from the kiln; too high a velocity will waste electrical energy for operating fans and impose unnecessary wear on the fan-motor-shaft system (Simpson 1991). Finding out the optimum values will be part of future work.

- 4) The wood drying model is valid for several usual species only. For the application of the program to other species, a database on the various physical properties of the wood has to be created.
- 5) The initial moisture content of the lumber pieces has been assumed to be the same and uniform. However, green wood has a wide variation of initial moisture content from pith to bark and different species may be dried together, which makes drying difficult. A method for grouping species, which is based on a mathematical model that estimates drying time in relationship to specific gravity, initial moisture content, temperature, equilibrium moisture content (EMC) and thickness [48], might be used together with the integrated model.
- 6) In order to validate and improve the models, we will have to set up experiments and compare numerical results with experimental data.

Appendix: Coefficients and Property Correlations

$$D_M^L = -\frac{\rho_L}{\rho_0} \frac{K_L K_{rL}}{\mu_L} \left(\frac{\partial P_c}{\partial M} \right)_T$$

$$D_T^L = -\frac{\rho_L}{\rho_0} \frac{K_L K_{rL}}{\mu_L} \left(\frac{\partial P_c}{\partial T} \right)_M$$

$$D_P^L = \frac{\rho_L}{\rho_0} \frac{K_L K_{rL}}{\mu_L}$$

Where ρ_i ($i = L, 0$) is density of liquid and oven-dry wood, respectively. K_L is the intrinsic permeability, and K_{rL} is the relative permeability. P_c is the capillary pressure. μ is the dynamic viscosity.

$$D_M^V = \frac{1}{\rho_0} \frac{D_{eff}}{RT} \frac{M_a M_v}{M} \left(\frac{\partial P_v}{\partial M} \right)_T$$

$$D_T^V = \frac{1}{\rho_0} \frac{D_{eff}}{RT} \frac{M_a M_v}{M} \left(\frac{\partial P_v}{\partial T} \right)_M$$

$$D_P^V = \frac{\rho_v}{\rho_0} \frac{K_g K_{rg}}{\mu_g} - \frac{1}{\rho_0} \frac{D_{eff}}{RT} \frac{M_a M_v}{M} \frac{P_v}{P}$$

$$D_P^a = \frac{\rho_a}{\rho_0} \frac{K_g K_{rg}}{\mu_g} + \frac{1}{\rho_0} \frac{D_{eff}}{RT} \frac{M_a M_v}{M} \frac{P_v}{P}$$

Where D_{eff} is the effective diffusion coefficient, M_a , M_v are the molecular mass of air and vapor, respectively. M is the mean molecular mass of gaseous phase.

$$\alpha = \frac{\varepsilon M_a (1 - S_L)}{\rho_0 RT}$$

$$\beta = -\frac{\varepsilon M_a (1 - S_L)}{\rho_0 RT} \left[\left(\frac{\partial P_v}{\partial M} \right)_T + \rho_0 \frac{P - P_v}{\rho_L \varepsilon (1 - S_L)} \right]$$

$$\gamma = -\frac{\varepsilon M_a (1 - S_L)}{\rho_0 RT} \left[\left(\frac{\partial P_v}{\partial T} \right)_M + \frac{P - P_v}{T} \right]$$

$$S_L = \frac{\rho_0 M}{\rho_L \varepsilon}$$

Where ε is the porosity of the wood and S_L is the dimensionless liquid saturation or the fraction of the void space filled with water.

The values of the coefficients used in the simulation are also listed.

Porosity:

$$\varepsilon = 0.7$$

Density of dry wood:

$$\rho_0 = 500 \text{ kg/m}^3$$

Average heat capacity:

$$\rho \cdot c_p = \rho_0 (1113 + 4.85T + 4185X), \text{ where } T \text{ is temperature,}$$

X is moisture content.

Fibre Saturation Point:

$$X_{\text{fsp}} = 0.598 - T/1000$$

Capillary pressure:

$$P_c = \sigma \times 1.364 \times 10^5 (X - X_{\text{fsp}} + 1.2 \times 10^{-4})^{-0.63}, \text{ where } \sigma = 72 \text{ dyne/cm.}$$

Permeabilities:

$$K_L = 5 \times 10^{-17}, K_g = 3 \times 10^{-18}$$

Binary Diffusivity of Air-Water Vapor Mixture:

$$D_{AB} = 2.2 \times 10^{-5} \left(\frac{101,325}{P} \right) \left(\frac{T}{273.15} \right)^{1.75}$$

Latent Heat of Vaporization:

$$\Delta h_v = 2.792 \times 10^6 - 160(T) - 3.43(T^2)$$

Liquid Water Density:

$$\rho = 878.19 + 1.1242(T) - 2.4368 \times 10^{-3}(T^2)$$

Water Vapor Density:

$$\rho = 27.692 - 3.899 \times 10^{-1}(T) + 2.074 \times 10^{-3}(T^2) - 4.943 \times 10^{-6}(T^3) \\ + 4.46 \times 10^{-9}(T^4), T < 375K.$$

Liquid Water Viscosity:

$$\text{Log}_{10}(\mu) = -13.73 + 1828.0(T^{-1}) + 1.966 \times 10^{-2}(T) - 1.466 \times 10^{-5}(T^2)$$

Air Viscosity:

$$\mu = 4.06 \times 10^{-8}(T) + 6.36 \times 10^{-6}$$

Water Vapor Viscosity:

$$\mu = 3.80 \times 10^{-8}(T) - 1.57 \times 10^{-6}$$

Nomenclature

C_f	friction factor
C_p	specific heat capacity at constant pressure ($\text{J.Kg}^{-1}\text{K}^{-1}$)
D	diffusion coefficient (m^2s^{-1})
D_{eff}	effective diffusion coefficient (m^2s^{-1})
EMC	equilibrium moisture content
FSP	fibre saturation point
G	Gibbs free energy
g	gravitational constant
h	specific enthalpy (J.Kg^{-1})
h	heat transfer coefficient ($\text{W. m}^{-2}\text{K}^{-1}$)
h_m	mass transfer coefficient (m s^{-1})
h_s	latent heat of vaporization of bound water
h_v	latent heat of vaporization of free water
K	intrinsic permeability (m^2)
k	relative permeability
k	turbulent kinetic energy
M	moisture content
$\langle m \rangle$	rate of evaporation ($\text{Kg. m}^{-3}\text{s}^{-1}$)
P	pressure
R	universal gas constant
Re	Reynolds number
RH	relative humidity
Sc	Schmidt number
Sh	Sherwood number
T	temperature (K)
t	time (s)
u	velocity vector (m s^{-1})
X	moisture content
x	the x-direction in a Cartesian system

Greek Letters

α, β, γ abbreviation used in Appendix.

σ	surface tension
ε	void fraction
λ	thermal conductivity ($\text{W}\cdot\text{m}^{-1}\text{k}^{-1}$)
μ	dynamic viscosity ($\text{Pa}\cdot\text{s}$)
ρ	fluid density ($\text{Kg}\cdot\text{m}^{-3}$)
ν	kinematic viscosity of the fluid
τ	fluid stress tensor (Pa)
τ_{ij}	Reynolds stress tensor (Pa)
ψ	water potential

Subscripts

a	dry air
b	bound water
c	cellulose matter
c	capillary
cr	critical
db	dry-bulb temperature
eff	effective
g	gas (air + vapor)
ini	initial value ($t=0$)
l	liquid
s	sorption
s	solid phase
v	vapor
vs	vapor saturation
wb	wet-bulb temperature

Superscripts

- average value
- g intrinsic average over the gaseous phase
- l intrinsic average over the liquid phase

References

1. Alden, Harry A., "Softwoods of North America," Forest Products Laboratory, United States Department of Agriculture, Forest Service, 1997.
2. Arnaud, G., "Study of the Air Flow in a Wood Drier," *Drying Technology*, Vol. 9, No. 1, pp. 183--200 (1991).
3. Basset, K.H., "Sticker Thickness and Air Velocity," Proceedings Western Dry Kiln Clubs, 25th Annual Meeting, May 9-10 (1974).
4. Beard, J. N., H. N. Rosen and B. A. Adesanya, "*Temperature Distributions and Heat Transfer during the Drying of Lumber*," *Drying Technology*, 1(1), pp. 117-140, 1983-1984.
5. Bejan, Adrian, "Heat Transfer," John Wiley & Sons, Inc., (1993).
6. Choong, E. T. *et al.*, "Relationship of Capillary Pressure and Water Saturation in Wood," *Wood Science and Technology*, Vol. 23, pp. 139-150, 1989.
7. Cloutier, A. and Y. Fortin, "A Model of Moisture Movement in Wood Based on Water Potential and the Determination of the Effective Water Conductivity," *Wood Science and Technology*, Vol. 27, pp. 95-114, (1993).
8. Cloutier, A. and Y. Fortin, "Moisture Content - Water Potential Relationship of Wood from Saturated to Dry Conditions," *Wood Science and Technology*, Vol. 25, pp. 263-280, (1991).
9. Cloutier, A., Y. Fortin, and G. Dhatt, "A Wood Drying Finite Element Model Based on the Water Potential Concept," *Drying Technology*, Vol. 10, No 5, pp. 1151-1181, (1992).

10. Comstock, G. L. *et al.*, "Factors Affecting Permeability and Pit Aspiration in Coniferous Sapwood," *Wood Science and Technology*, Vol. 2, pp. 279-291, 1968.
11. Denig, Joseph, Eugene M. Wengert and William T. Simpson, "Drying Hardwood Lumber," Forest Products Laboratory, United States Department of Agriculture, Forest Service, 2000
12. Esfahanian, A. Hashemi, "Numerical Investigation of Fluid Flow and Heat/Mass Transfer Over a Stack of Planks," *CSME Forum SCGM*, Vol. 1, pp. 345-350, 1998.
13. Ferguson, W. J. and I.W. Turner, "A Comparison of the Finite Element and Control Volume Numerical Solution Techniques Applied to Timber Drying Problem Below the Boiling Point," *Int. J. for Numerical Methods in Engineering*, Vol. 38, pp. 451-467, (1995).
14. Forest Products Laboratory, Dry Kiln Operator's Handbook, Forest Services, U.S. Department of Agriculture, (1988).
15. Gong, Li and O.A. Plumb, "The Effect of Heterogeneity on Wood Drying, Part I: Model Development and Predictions," *Drying Technology*, 12(8), pp. 1983-2001, (1994).
16. Gong, Li and O.A. Plumb, "The Effect of Heterogeneity on Wood Drying, Part II: Experimental Results," *Drying Technology*, 12(8), pp. 2003-2026, (1994).
17. He, P., M Salcudean, I.S. Gartshore and P. Nowak, "Multigrid Calculation of Fluid Flows in Complex 3D Geometries Using Curvilinear Grids," *Computers and Fluids*, Vol. 25, No. 4, pp. 395-419 (1996).

18. Hua, Lu, Eric Bibeau, P. He, I.S. Gartshore, and M. Salcudean, "Modelling of Airflow in Wood Kilns (Airflow 101)," *Wood Technology Clinic*, Portland, Oregon, March 25-27, 1998.
19. Ilic, M. and I.W. Turner, "Convective Drying of a Consolidated Slab of Wet Porous Material," *Int. J. Heat and Mass Transfer*, Vol. 32, No. 12, pp. 2351-2362, (1989).
20. Kamke, Frederick A. and Manfred Vanek, "Comparison of Wood Drying Models," 4th IUFRO International Conference on Wood Drying, Rotorua, New Zealand, 1994.
21. Kho, P.C.S., R.B. Keey and J.C.F. Walker, "Effects of Minor Board Irregularities and Air Flows on the Drying Rate of Softwood Timber Boards in Kilns," IUFRO, Wood Drying, pp. 150-157 (1989).
22. Langrish, T.A.G., P.C.S. Kho, R.B. Keey and J.C.F. Walker, "Experimental Measurements and Numerical Simulation of Local Mass Transfer Coefficients in Timber Kilns," *Drying Technology*, Vol. 10, No. 3, pp. 753--781 (1992).
23. Langrish, T.A.G., R.B. Keey, P.C.S. Kho and J.C.F. Walker, "Time-Dependent Flow in Arrays of Timber Boards: FLOW Visualization, Mass-Transfer Measurements and Numerical Simulation," *Chemical Engineering Science*, Vol. 48, No. 12, pp. 2211-2223, (1993)
24. Leverett, M.C., "Capillary Behavior in Porous Solids," *AIME Transactions*, Vol. 142, pp. 152-169 (1941).
25. Luikov, A.V., Heat and Mass Transfer in Capillary-Porous Bodies, Pergamon Press, New York, pp. 233-255, (1966).

26. Mackay, J.F.G. and L.C. Oliveira, Kiln Operator's Handbook for Western Canada, Forintek Canada, SP-31, ISSN 0824-2119 (1989).
27. Message Passing Interface Forum. MPI-2: Extensions to the Message-Passing Interface, 1997. <http://www.mpi-forum.org>.
28. Milota, Michael R. and John L. Tschernitz, "Simulation of Drying in A Batch Lumber Kiln from Sigle-Board Tests," *Drying Technology*, 12(8), pp. 2027-2055, 1994.
29. Nasrallah, S. Ben and P. Perre, "Detailed Study of a Model of Heat and Mass Transfer During Convective Drying of Porous Media," *Int. J. Heat and Mass Transfer*, Vol. 31, No. 5, pp. 957-967, (1988)
30. Pang, Shusheng and A.N. Haslett, "The Application of Mathematical Models to the Commercial High-Temperature Drying of Softwood Lumber," *Drying Technology*, Vol. 13, No. 8&9, pp. 1635-1674, (1995).
31. Pang, Shusheng, "External Heat and Mass Transfer Coefficients for Kiln Drying of Timber," *Drying Technology*, Vol. 14, No. 3&4, pp. 859-871, (1996).
32. Pang, Shusheng, T.A.G. Langrish and R.B. Keey, "Moisture Movement in Softwood Timber at Elevated Temperatures," *Drying Technology*, Vol. 12, No 8, pp. 1897-1914, (1994).
33. Perre, P. and C. Moyne, "Process Related to Drying: Part I, Theoretical Model" *Drying Technology*, Vol. 9, No 5, pp. 1135-1152, (1991).
34. Perre, P. and C. Moyne, "Process Related to Drying: Part II, Use of the Same Model to Solve Transfers both in Saturated and Unsaturated Porous Media," *Drying Technology*, Vol. 9, No 5, pp. 1153-1179, (1991).

35. Perre, P. and Degiovanni, "Simulation par Volume Finis des Transferts Couplés en Milieux Poreux Anisotropes: Séchage du Bois a Basse et a Haute Temperature," *Int. J. Heat and Mass Transfer*, Vol. 33, No. 11, pp. 2463-2478, (1990).
36. Perre, P. and M. Martin, "Drying at High Temperature of Sapwood and Heartwood: Theory, Experiment and Practical Consequence on Kiln Control," *Drying Technology*, Vol. 12, No 8, pp. 1915-1941, (1994)
37. Perre, P., J.P. Fohr, and G. Arnaud, "A Model of Drying Applied to Softwoods: The Effect of Gaseous Pressure Below the Boiling Point," *Drying 89*, Hemisphere, Washington, D.C., pp. 91-98, (1989).
38. Perre, P., M. Moser and M. Martin, "Advances in Transport Phenomena During Convective Drying with Superheated Steam and Moist Air," *Int. J. Heat and Mass Transfer*, Vol. 36, No. 11, pp. 2725-2746, (1993).
39. Plumb, O. A., G. A. Spolek and B. A. Olmstead, "Heat and Mass Transfer in Wood During Drying," *Int. J. Heat and Mass Transfer*, Vol. 28, No. 9, pp. 1669-1678, (1985).
40. Rice, Robert W. *et al.*, "Kiln Drying Lumber in the United States: A Survey of Volumes, Species, Kiln Capacity, Equipment, and procedures, 1992-1993," Forest Products Laboratory, Madison, Wisconsin, 1994.
41. Rietz, Raymond C. and Rufus H. Page, "Air Drying of Lumber," Madison, WI: U.S. Department of Agriculture, Forest Service, Forest Products Laboratory, 1999.
42. Rosen, H.N., "Recent Advances in the Drying of Solid Wood," *Advances in Drying*, Volume 4, A.S. Mujumdar Editor, pp. 99-147, (1986).
43. Siau, J. F., "Flow in Wood," Syracuse University Press, N. Y. 1971.

44. Simpson, William T. and H. N. Rosen, "Equilibrium Moisture Content of Wood at High Temperature," *Wood and Fibre*, 13(3), pp150-158, 1981.
45. Simpson, William T., "Dry kiln operator's manual," Washington, DC: U.S. Department of Agriculture. P. 274, (1991).
46. Simpson, William T., "Drying Wood: A Review – Part I," *Drying Technology*, 2(2), pp. 235-264, 1983-1984.
47. Simpson, William T., "Equilibrium Moisture Content Prediction for Wood," *Forest Product Journal*, 21(5), pp. 48-49, 1971.
48. Simpson, William T., "Grouping Tropical Wood Species for Kiln Drying Using Mathematical Models," *Drying Technology*, 12(8), pp. 1877-1896, (1994).
49. Sparrow, E.M., J.E. Niethammer, and A. Chaboki, "Heat Transfer and Pressure Drop Characteristics of Arrays of Rectangular Modules Encountered in Electronic Equipment," *Heat and Mass Transfer*, Vol. 25, No. 7, pp. 961-973, (1982)
50. Spoleck, G. A. and O. A. Plumb, "Capillary Pressure in Softwood," *Wood Science and Technology*, Vol. 15, pp. 189-199, 1981.
51. Spolek, G.A. and O.A. Plumb, "A Numerical Model of Heat and Mass Transport in Wood During Drying," *Drying 80*, Hemisphere, Washington, D.C., pp. 84-92, (1980).
52. Stamm, A.J. and N.C. Raleigh, "Movement of Fluids in Wood – Part I: Flow of Fluids in Wood," *Wood Science and Technology*, Vol. 1, pp. 122-141, (1967).
53. Stanish, M.A., G.S. Schajer and Ferhan Kayihan, "Mathematical Model of Drying for Hygroscopic Porous Media," *AIChE Journal*, Vol. 32, No. 8, 1986.

54. Sugawara, S., T. Sato, H. Komatsu and H. Osaka, "Effect of Free Stream Turbulence on Flat Plate Heat Transfer," *Int. J. of Heat and Mass Transfer*, Vol. 31, No. 1, pp. 5-12, (1988).
55. Sutherland, J. W., I.W. Turner and R. L. Northway, "A theoretical and Experimental Investigation of the Convective Drying of Australian *Pinus Radiata* Timber", *Drying Technology*, 12(8), pp. 1815-1839, (1994).
56. Turner, I.W. and M. Ilic, "Convective Drying of a Consolidated Slab of Wet Porous Material including the Sorption Region," *Int. Comm. Heat Mass Transfer*, Vol. 17, pp. 39-48, (1990).
57. Whitaker, S., "Heat and Mass Transfer in Granular Porous Media," *Advances in Drying*, Vol. 1, pp. 23-61, 1980.
58. Whitaker, S., Simultaneous heat and momentum transfer in porous media: a theory of drying, *Advances in Heat Transfer*, Vol. 13, 119-203, Academic Press, N.Y. (1977).
59. White, F.M., "Viscous Fluid Flow," ISBN 0070697124, McGraw-Hill, New York, NY, (1991).
60. Wu, Q., A.R. Oliver, and P.E. Doe, "A Study of the Boundary Layer Flow Through a Lumber Drying Stack," *Drying Technology*, Vol. 13, No. 8&9, pp. 2011--2026 (1995).